2009

MUTAGENESIS AND SPECTROSCOPIC STUDIES OF MYCOBACTERIUM TUBERCULOSIS STEROL 14ALPHA DEMETHYLASE.

Anuja R. Modi
Virginia Commonwealth University

MUTAGENESIS AND SPECTROSCOPIC STUDIES OF MYCOBACTERIUM TUBERCULOSIS STEROL 14ALPHA DEMETHYLASE.

A thesis submitted in partial fulfillment of the requirements for the degree of Master of Science at Virginia Commonwealth University.

by

ANUJA RATNAKAR MODI
Bachelor of Pharmaceutical Sciences, Mumbai University, India, 2007

Director: JOHN C HACKETT, PHD,RPH
ASSISTANT PROFESSOR OF MEDICINAL CHEMISTRY.

Virginia Commonwealth University
Richmond, Virginia
August, 2007.

Acknowledgement

I would sincerely like to thank my adviser Dr. John Hackett for his unconditional support during the course of my Masters education. He practically let me have the lab for myself and thanks to this freedom and encouragement I was able to learn so much. During our long and wide ranging conversations I learned a lot about P450 enzymology and catalysis. I really admire his patience and his zest for food! Dr. Hackett has been a friend, a philosopher and a guide for the past one and half year and I will surely miss him as I embark on my next journey in Columbia, SC. I am extremely glad and lucky to have him as my adviser. I am grateful to Dr. Krishna Iyer, my professor from Bombay College of Pharmacy who instigated my 'love affair' with P450s, which continues as I go for PhD.

I would also like to thank Dr. James Terner and Dr. Jason Rife for being on my committee. I am especially thankful to Dr. James Terner for helping us in recording resonance Raman spectra, for his time, patience, photos and Japanese learning tips. I would like to thank our lab members Dr. Kakali Sen, Gareth Jennings, Justin Elewenski and Shahenda. They are all very nice, have a great sense of humor and they made lab a fun place to be! I am indebted to Kakali for her time and patience in helping me with principles of computational quantum chemistry and resonance Raman. She is a great

person, someone whom I will always look up to. I am very thankful to Gareth as well for helping me with the recording of resonance Raman spectra.

I am thankful to all those working here in the Institute of Structural Biology and Drug Discovery. This is a great place to work and a true shared resource institute; I don't remember a single lab from where I haven't borrowed things! I would like to thank Dr Martin Safo in whose lab I learned cloning, Dr. Darrell Peterson and Mario for their help with cloning and protein purification, Pooja for helping me with site directed mutagenesis and Rami, Jenson and Jay for helping me with synthesis of dihydrolanosterol. I am also thankful to Juni for introducing me to ligation independent cloning, Dr. David Williams and Ninad for allowing us to use their FPLC, Dr. Keith Ellis for being the Dean's representative for my defense and allowing us to use his GeneVac and Deboleena for helping me with the LC. I would like to specially mention Sharon Lee and Michelle Craighead for all their help. I would also like to mention all my friends here at the institute and in Medicinal Chemistry, Maria, Zohal, Bijoy, Tamara, Soumya, Sayali, Jigar, Aiye, Ashutosh, Arjun, Pooja, Arpan Jay, Preetpal, Jitesh, Hardik, Mohini, Vishal and Tim, thanks to you all it was great fun working here and I am going to miss each and every one of you.

I am extremely grateful to my cousin Amey and my best friend Juee for just being there for me. I would also like to specially mention my friends and roommates for being a family away from home, for their love, emotional support especially in difficult times and

for giving me unforgettable memories of Richmond and Berkshire, Harsha, Spandana, Ritesh, Devnath, Tejas, Shyam, Aditya, Sirisha, Deepa, Aditi, Sudarshana, Khusbsoo and Alpana.

Above everything I would like to thank my family, Mom and my brother Amit for their love, constant support and encouragement. Words cannot express the gratitude I feel for them. On this day the only thing amiss is my Dad's presence and I so wish he was here today. He continually and convincingly conveyed a spirit of hard work, perseverance and enthusiasm without which I would have never made it.

And last but not the least I would like to thank the Department of Medicinal Chemistry, and School of Pharmacy at VCU for giving me this wonderful opportunity to study here.

In the loving memory of my Dad, miss you.

.

Table of Contents

List of Tables

Page

List of Figures

Page

Abstract

MUTAGENESIS AND SPECTROSCOPIC STUDIES OF MYCOBACTERIUM TUBERCULOSIS STEROL 14ALPHA DEMETHYLASE

By Anuja Ratnakar Modi, B. Pharm. Sci.,

A thesis submitted in partial fulfillment of the requirements for the degree of Master of Science at Virginia Commonwealth University.

Virginia Commonwealth University, 2009

Major Director: John C. Hackett, PhD, RPh.
Assistant Professor, Department of Medicinal Chemistry.

P450s are heme containing enzymes which affect oxidation of substrates via catalytic intermediates having transient lifetimes. These oxidative catalytic intermediates are formed by a sequential interplay of electrons and protons at the active site of the enzyme bearing molecular dioxygen. The proton transfer to the active site from bulk solvent is coordinated by an "acid-alcohol" pair of active site residues which are conserved in all P450s. Sterol 14α-demethylases (CYP51) are P450 enzymes which catalyze oxidative deformylation of lanosterol in the cholesterol/ergosterol biosynthetic pathway. Both cholesterol and ergosterol are important regulators of membrane fluidity. CYP51

differs from other P450s in that the acid in the acid-alcohol pair in the active site is replaced by a His residue.

This enzyme is present in tuberculosis (TB) causing pathogen *Mycobacterium tuberculosis* (Mtb). This finding was significant for primarily two reasons. The first one being the baffling presence of CYP51 in Mtb, as Mtb is not known to have any endogenous sterol biosynthetic pathways. The second being that CYP51 is a validated drug target in treating fungal infections. Thus given the global resurgence of multidrug resistant strains of Mtb and the deadly coexsistence of Mtb in immunocompromised HIV patients, CYP51 may be an ideal drug target for new generation of antimycobacterial drugs.

The Mtb CYP51 enzyme was chosen to study the proton transfer pathways in the active site based on the outcome of explicit solvent molecular dynamics and hybrid quantum mechanics/molecular mechanics calculations performed in our laboratory. Based on these calculations of CYP51 catalysis, Glu173 was implicated to be the proton source. Proton transfer to the active site occurred by a coordinated shuttling via four water molecules, His259 and Thr260. To experimentally verify the roles of Glu173, His259 and Thr260 they were mutated to alanine and biophysically characterized. Ferredoxin, an accessory protein required to shuttle electrons from NADPH to the CYP51 active site for catalysis, was also cloned using ligation independent cloning.

We were successfully able to reconstitute the electron transport chain for CYP51. The mutants were found to differentially bind type I and type II enzymes. Based on biophysical characterization, Thr260 can be implicated to have a role in modulating the spin state of the enzyme.

CHAPTER 1: BACKGROUND

1.1 Introduction

Cytochrome P450s (P450s) belong to the heme containing monoxygenase family of enzymes. These are heme *b*-containing enzymes in which the iron protoporphyrin IX macrocycle (Figure 1) is non-covalently attached to the protein and the heme iron is axially coordinated by a cysteine thiolate. They are some of the most versatile oxidants found in nature. P450s are so called because the carbonmonoxy ferrous enzymes have a characteristic Soret absorbance at 450 nm. These enzymes affect functionalization of molecules using O_2 along with a diverse set of redox partners. The resulting product thus contains either one or both atoms of the oxygen molecule.[1] P450s are found throughout the biological domains and their functions can be generally classified into two roles. The first one is in metabolism of xenobiotics to aid their removal from the body and a second functional role is in biosynthesis of intermediates used for development and homeostasis.[2,3] They are also responsible for degradation of more than 70% of the clinically available drugs and those in the drug development pipeline.

P450s catalyze a host of different chemical reactions.[4] They are however well known for their ability to efficiently hydroxylate unactivated C-H bonds. The catalytic mechanism of P450 occurs in a cyclic fashion putatively involving eight transient intermediates, some

of them being very short-lived caged radical pairs.[5] It also involves interaction with protein redox partners which shuttle electron to the P450s from reducing equivalents, provided by nicotinamide adenine dinucleotide (phosphate) (NAD(P)H)in most cases (Figure 3).[6,7]

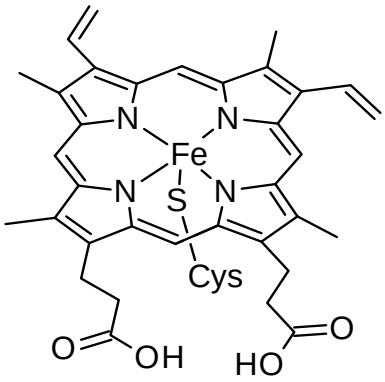

Figure 1: Iron protoporphyrin IX macrocycle with cysteine thiolate as an axial ligand.

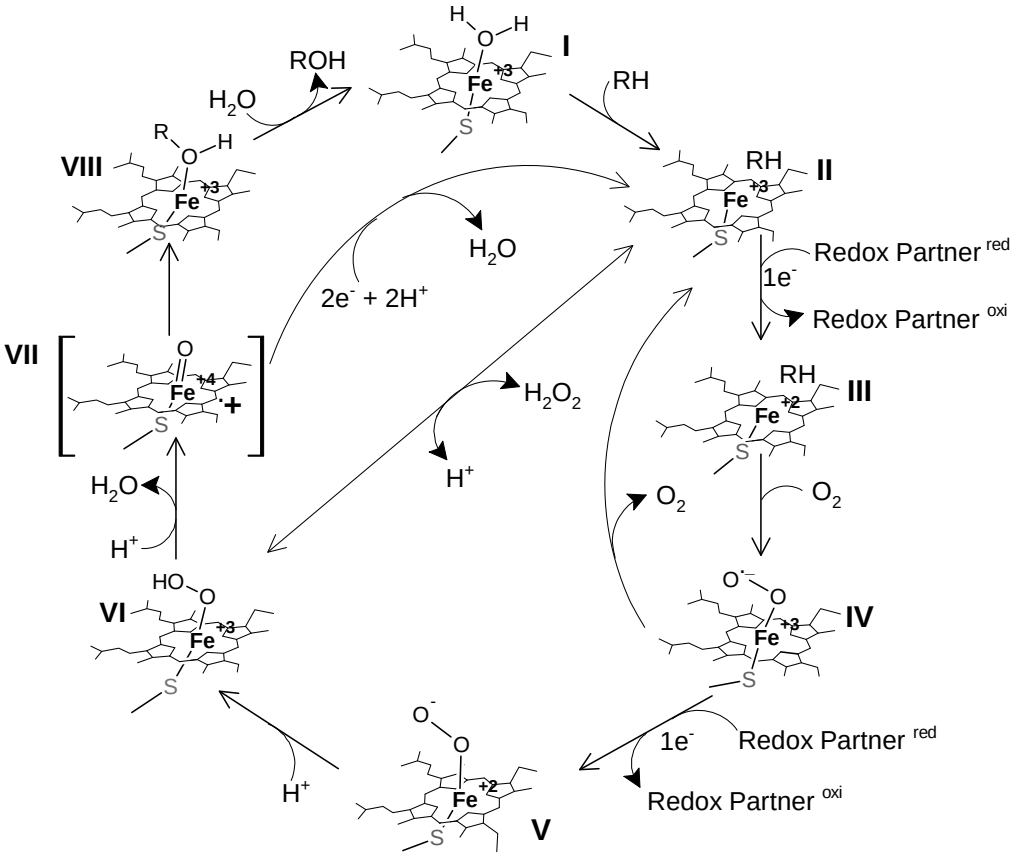

Figure 2: Catalytic cycle of cytochrome P450

1.2 Catalytic cycle of P450

The catalytic cycle begins with substrate binding to the water-coordinated low spin (S=1/2) resting state of ferric enzyme [Figure 2 1**,I**]. Substrate binding causes displacement of water as the sixth ligand of heme and formation of high-spin (S=5/2) penta coordinate enzyme substrate adduct [Figure 2, **II**].[8] This causes the midpoint redox potential of the heme to shift to a more positive value.[9] The ultimate electron donor, NAD(P)H and its associated redox partners have roughly similar low redox midpoint potentials. Thus the sharp shift in the reduction potential resulting from substrate binding causes two electrons to flow from NAD(P)H to the P450 via an associated reductase, the first one of which generates the reduced ferrous substrate adduct [Figure 2, **III**].[9] Subsequent binding O_2 generates an oxyferrous complex [Figure 2, **IV**]. The second electron from NAD(P)H then reduces the oxyferrous complex resulting in the Fe^{+3}-OO^{2-} [Figure 2, **V**] peroxo-ferric intermediate. Protonation of this intermediate leads to the Fe^{+3}-OOH [Figure 2, **VI**] hydroperoxo-ferric intermediate, also known as Compound 0 (Cmpd 0). This is the last intermediate in the catalytic cycle which has been characterized using spectroscopic techniques.[10,11] A second protonation of this intermediate leads to O-O bond lysis forming the highly transient and reactive oxo ferryl porphyrin π radical cation complex [Figure 2, **VII**] also known as Compound I (Cmpd I). Cmpd I is one of the most powerful oxidants in biology, causing substrate oxidation by the commonly accepted hydrogen atom abstraction-hydroxyl radical rebound mechnism.[12,13] The enzyme then returns to its resting state.

In addition to the normal cycle, there are three uncoupling reactions within the cycle which lead to the enzyme substrate adduct [Figure 2, **II**].[14] The first one is the auto-oxidation of the oxyferrous enzyme [Figure 2, **IV**] with simultaneous generation of a superoxide anion. The second one is where the hydroperoxo anion dissociates from the hydroperoxo ferric intermediate [Figure 2, **VI**], liberating hydrogen peroxide and leading to cycle completion, however the substrate turnover is incomplete. In the oxidase shunt the oxoferryl intermediate [Figure 2, **VII**] is oxidized to water in lieu of substrate oxidation.

Given the important metabolic role, the varied and unusual nature of chemistry (oxidation of unactivated alkanes at room temperature and physiological pH) carried out by P450 enzymes; they have attracted attention from pharmacologists, organic, inorganic and physical chemists alike. The mechanistic elucidation of these enzymes, particularly O_2 activation, proton transfer pathways and isolation of intermediates remain among the most researched and debated areas. Most studies have used iron protoporphyrin IX macrocycle mimetics, substrate analogs, spectroscopic studies and molecular biology techniques. Comparison of P450 enzymes with other similar heme containing, oxidizing enzymes like peroxidases,[16] catalases, heme oxygenases,[17] and nitric oxide synthases[18] have given insight into their mechanism.

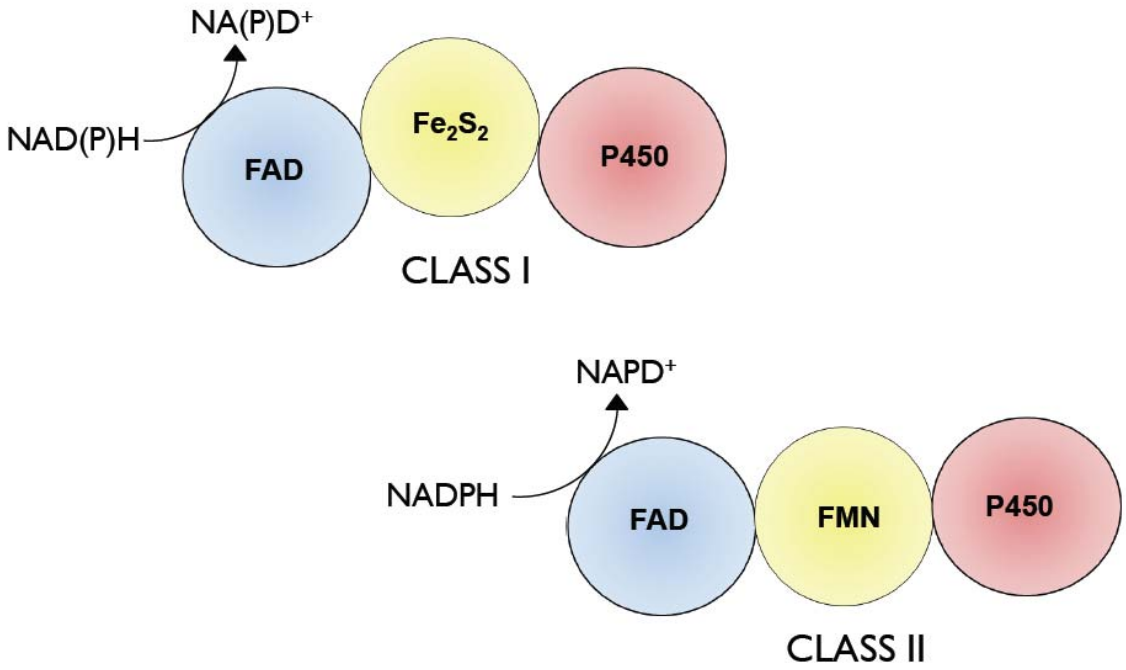

Figure 3: P450s and their associated redox systems.[15] Type I systems use a FAD containing ferredoxin reductase and an iron-sulfur containing ferredoxin to shuttle electrons to P450 from NAD(P)H. Type II systems utilize a diflavin (FAD and FMN) containing membrane bound NADPH cytochrome P450 reductase to shuttle electrons to P450s.

1.3 Active site structure of P450s

The overall structure of P450s is conserved and made up of four-helices, three of which are parallel D, L and I while helix E is antiparallel.[15] The heme group is confined between the I-helix on the distal side and L helix on the proximal side and is bound to the adjacent Cys-ligand-loop (Figure 4 A), containing the signature P450 sequence 'FxxxGx(H/R)xCxG' (black dashed box, Figure 5). The sulfur thiolate of the cysteine is the proximal ligand to the heme iron and is responsible for the characteristic Soret absorbance at 450 nm.[19] It is absolutely conserved in all P450s (highlighted in red in Figure 5). Water forms distal ligand in the resting state of the enzyme.

The I helix traverses across the active site and contains the conserved sequence '(A/G)Gx(E/D/H)T' (red dashed box, Figure 5) centered at a kink over the heme. A primary structure alignment of P450s reveals a conserved acid-alcohol pair in the active site (highlighted in blue in Figure 5, Figure 4 B).[20] The alcohol residue is typically threonine or serine and the acid residue being aspartate or glutamate. The alcohol residue is implicated in the key role of proton source for the peroxo species and/or stabilizing hydrogen bond and water molecule network for proton delivery and O-O bond scission.[21] Mutations in the acid residue result in decreased catalytic turnover of the enzyme.[22] Subsequent investigations have suggested its role in second electron transfer and further events leading to Cmpd I formation.[23]

A)

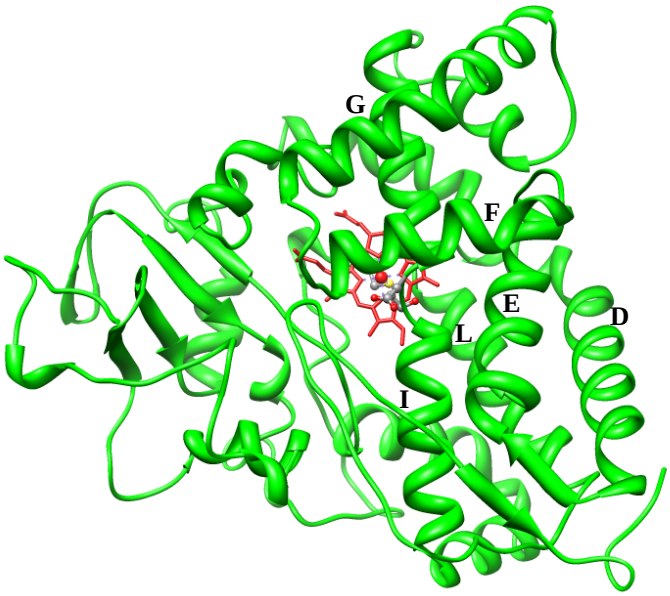

B)

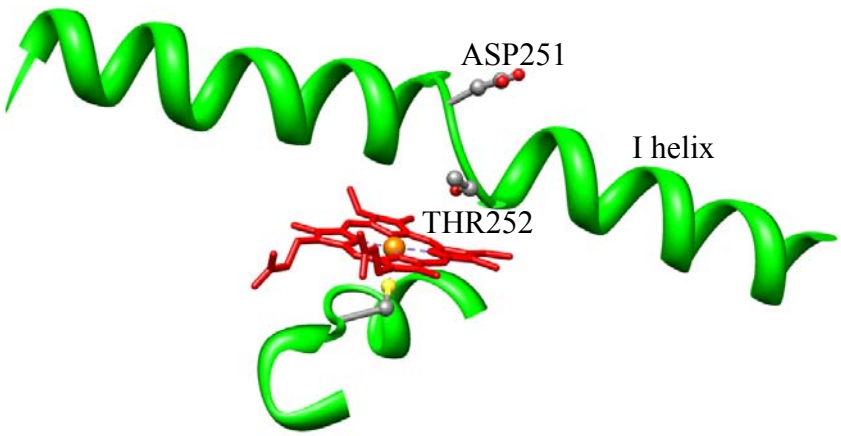

Figure 4: The structures of a typical P450 showing A) over all fold of P450cam (PDB code 1AKD)[24], a camphor monoxygenase from *Pseudomonas putida*, with helices labeled and B) active site structure showing the heme, the cysteine thiolate ligand and the conserved acid-alcohol (Asp251-Thr252) pair in the I helix.

Figure 5: Sequence alignment of bacterial P450s, CYP101 (green; PDB 1AKD)-P450cam from *Pseudomonas putida*,[24] CYP51 (pink; PDB 1H5Z)-lanosterol 14α-demethylase from *Mycobacterium tuberculosis*,[25] CYP119 (yellow; PDB 1IO9)-P450 from acidothermophilic archaeon *Sulfolobus solfataricus*,[26] CYP102 (blue; PBD 1N40)- a fatty acid monoxygenase from *Bacillus megaterium*.[27] Dashed boxes show the conserved sequences and highlighted amino acids are the conserved residues.

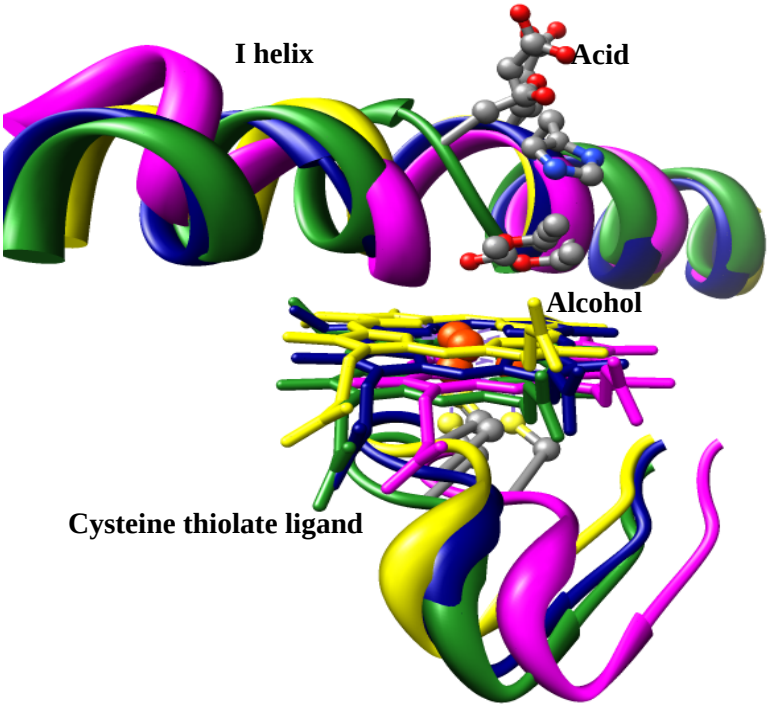

Figure 6: Structural alignment of bacterial P450s, CYP101 (green) -from *Pseudomonas putida*, CYP51 (pink)-lanosterol 14α-demethylase from *Mycobacterium tuberculosis*, CYP119 (green)-from acidothermophilic archaeon *Sulfolobus solfataricus*, CYP102 (blue)- a fatty acid monoxygenase from *Bacillus megaterium*, showing the conserved acid-alcohol pair and the cysteine thiolate ligand.

1.4 *Mycobacterium tuberculosis* and Tuberculosis

Mycobacterium tuberculosis (Mtb) is a pathogenic bacterium that causes the contagious disease Tuberculosis (TB). It is an obligate aerobe that establishes itself in the alveolar macrophages of the lung in the initial stages of infection. Eventually it spreads out to other tissues in the body such as bones, joints and skin via blood. The disease TB is so called due to formation of characteristic cellular structures in the body called tubercles in which the Mtb bacilli thrive, protected from surroundings. Mtb is not only able to survive host immune responses, but also continue living and duplicate in alveolar macrophages, unlike most pathogenic bacteria.[28] Mtb's cellular structure and its ability to modify both, its own and the host's cell membrane contribute greatly to its virulence. The cell envelope of Mtb is extremely complex with an additional layer rich in unusual lipids, polyketides, glycolipids and polysaccharides (Figure 7).[29]

TB was once thought to be virtually eradicated in developed countries due to development of novel antimycobacterial drugs and improved public health management. However with recent resurgence of multi-drug resistant (MDR) strains of Mtb and the immunocompromising nature of HIV virus allowing TB to thrive and spread in the host make the statistics associated with TB frightening (Figure 8). This has led to World Health Organization (WHO) recognizing TB as a potential global emergency for human health (WHO publication no. WHO/TB/94.177). After the discovery of the first anti-tubercular drug streptomycin in 1943, followed by isoniazid, para-amino salicylic acid and rifampicin in the early 1960s, the drug regime for TB has remained unchanged for the past 50 years.[30] The widespread emergence of MDR Mtb strains to long used antimycobacterial drugs

indicates the urgent need for new anti TB drugs and subsequent discovery of novel drug targets in Mtb.

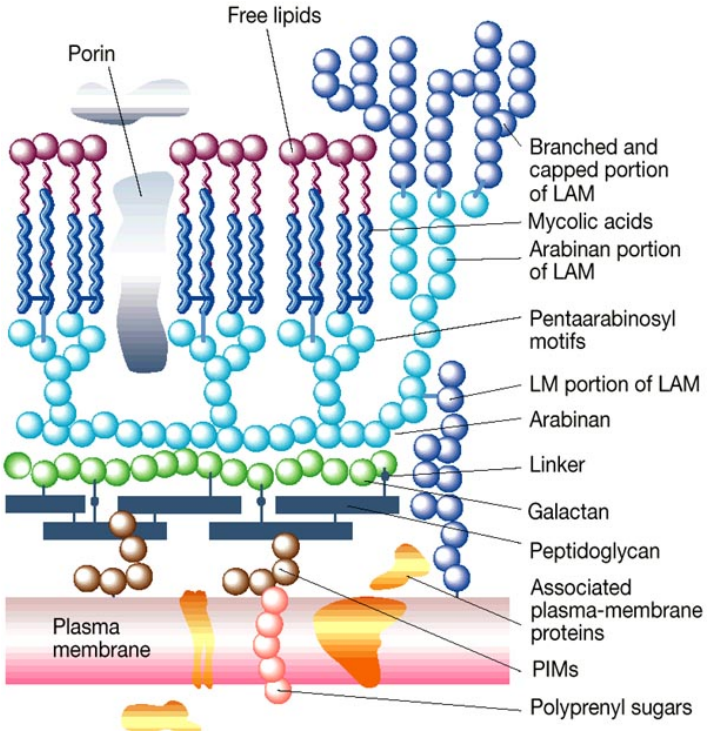

Figure 7: Lipid rich cell wall of Mtb, LAM, lipoarabinomannans; LM, lipomannans; PIM, phosphatidylinositol mannosides.[31]

1) Estimated number of new TB cases, by country, 2007

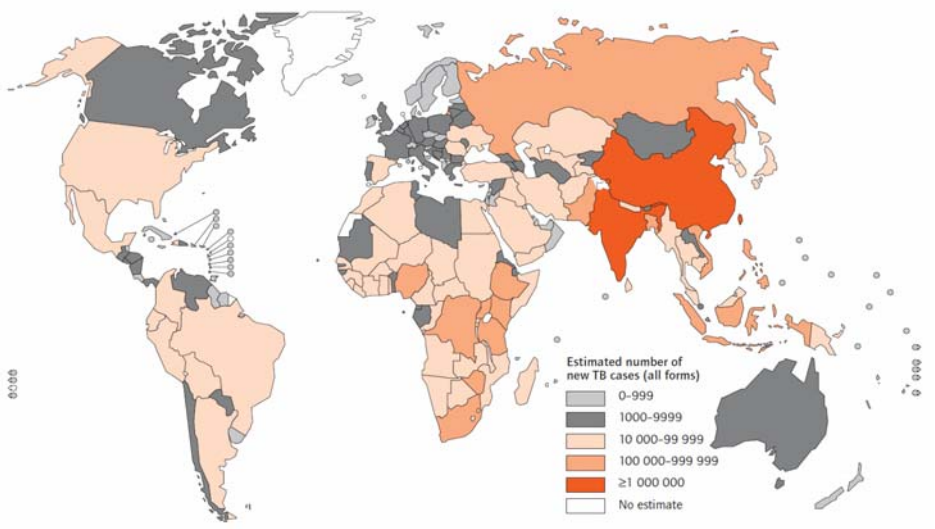

2) Estimated HIV prevalence in new TB cases, 2007

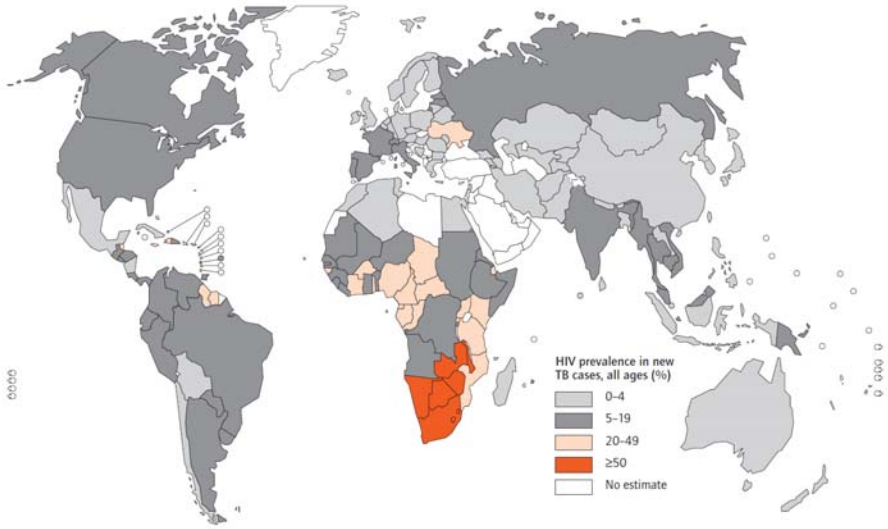

Figure 8: Statistics associated with TB**.** Data from WHO TB report 2009 (WHO/HTM/TB/2009.411)

1.5 P450s in Mtb

The complete genome sequencing of Mtb by Stewart Cole and coworkers in 1998 was an important step in helping to decipher Mtb's biology.[32] A surprising revelation in the clinically virulent strain of Mtb H37Rv was the presence of twenty different Cytochrome P450 genes (CYPs). While in eukaryotic systems P450 enzymes are essential for lipid metabolism and are clinically proven antifungal targets, for a prokaryotic organism twenty P450s was an unexpectedly large number. For instance in humans there are 57 P450's in a genome of ~3.3 billion meaning approximately 1 P450/5.8 million bp, but in Mtb it is 1 P450/220,000 bp of the genome (Cytochrome P450 homepage at http://drnelson.utmem.edu/CytochromeP450.html) However, a large number of oxidase enzymes complements the obligate aerobic nature of Mtb and given the lipid rich nature of Mtb pathogen and a potential for these P450s to serve as novel antitubercular targets, their structure/function characterization would open up new areas in TB therapy.[33] To date, crystal structures of three Mtb P450s have been published (Figure 9), CYP51[25], CYP121[34] and CYP130[35]. CYP51 is a sterol 14α-demethylase enzyme which catalyzes the 14α-demethylastion of lanosterol (in mammals/fungi) and obtusifoliol (in plants) in the pathway leading to cholesterol (in mammals) and ergosterol (in plants/fungi) both being important regulators of membrane fluidity.[36] The functions of CYP121 and CYP130 remain unknown. Table 1 lists the putative P450 genes of which possible functions are known.[37] Since the Mtb genome was sequenced, the presence of CYP51 has gathered considerable interest for two reasons, is its baffling presence in Mtb which lacks a sterol

biosynthetic pathway and for the fact that it is a validated clinical target in anti-fungal therapy.

Table1: Mtb H37Rv CYPs and their possible functions

CYP	Gene	Key facts/possible function
CYP51	*Rv0754c*	Sterol 14α-demethylase[38,39], possible role in host sterol inactivation.[39]
CYP121	*Rv2276*	Putative essential gene, possible role in virulence.[40]
CYP123	*Rv0766c*	Upregulated at high temperatures.[41]
CYP125	*Rv3545c*	Induced in macrophages, essential for infection in mice.[42]
CYP128	*Rv2268c*	Possible essential gene, required for Mtb growth in-vitro.[43]
CYP130	*Rv1256c*	Adjacent to an oxidoreductase.[35]
CYP132	*Rv1394c*	Possible role in Mtb virulence. Similar to fatty acid metabolizing P450s.
CYP138	*Rv0136*	Upregulated at high temperatures.[41]
CYP141	*Rv3121*	Surrounding genes involved in molybdenum co-factor biosynthesis
CYP144	*Rv1777*	Possible role in virulence.

A)

B)

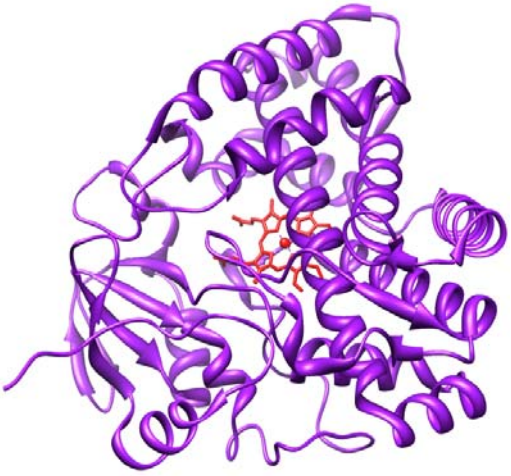

C)

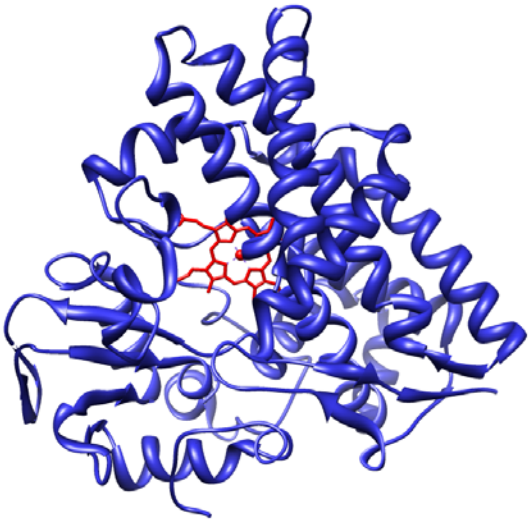

Figure 9: Structures of Mtb P450s A)CYP51(PDB code 1H5Z), B)CYP121(PDB code 3G5F) and C)CYP130(PDB code 2UUQ).

In my thesis here I will describe investigations in the *Mycobacterium tuberculosis* P450 enzyme, sterol 14α-demethylase (CYP51) using site directed mutagenesis, UV-vis and resonance Raman spectroscopy, cloning and expression of a P450 accessory protein from Mtb Ferredoxin(Fdx) and cloning and trial expression of another P450 from Mtb, CYP132.

CHAPTER 2: Mutagenesis and Characterization of CYP51

2.1 Introduction

The CYP51 enzymes are found throughout the biological kingdoms and are one of the most ancient members of the P450 family.[44] CYP51 catalyzes the oxidative deformylation of lanosterol, concomitantly adding a double bond in three oxidative steps, each utilizing a single equivalent of NADPH and O_2 (Figure 10).[45,46] In the first step, the 14α-methyl group is oxidized to the corresponding alcohol. The alcohol in the next step is oxidized to a diol, which dehydrates to an aldehyde. The final step results in cleavage of the C14-C32 bond with stereoselective removal of 15α-H, resulting in the formation of a 14,15 double bond and release of formic acid. While the first two steps have been proposed to occur by Cmpd I-mediated hydrogen radical abstraction/hydroxyl radical rebound,[12,13] the last step is thought to be mediated by the peroxo species.[46] A primary sequence analysis of CYP51 enzymes reveals that the acid in the acid-alcohol is replaced by a His residue (Figure 5).[44]Conventionally, either an aspartic acid or a glutamic acid residue is found in this position. When the X-ray crystal structure of Mtb CYP51 is compared with those of other P450's, it is revealed that this dyad occupies the same position as the conventional acid-alcohol pair in the active site of other P450s (Figure 6). This unusual replacement raises

questions as to how O_2 is activated in CYP51 and the subsequent modulation of the lifetimes of intermediates in the catalytic cycle involved in oxidative biotransformation.

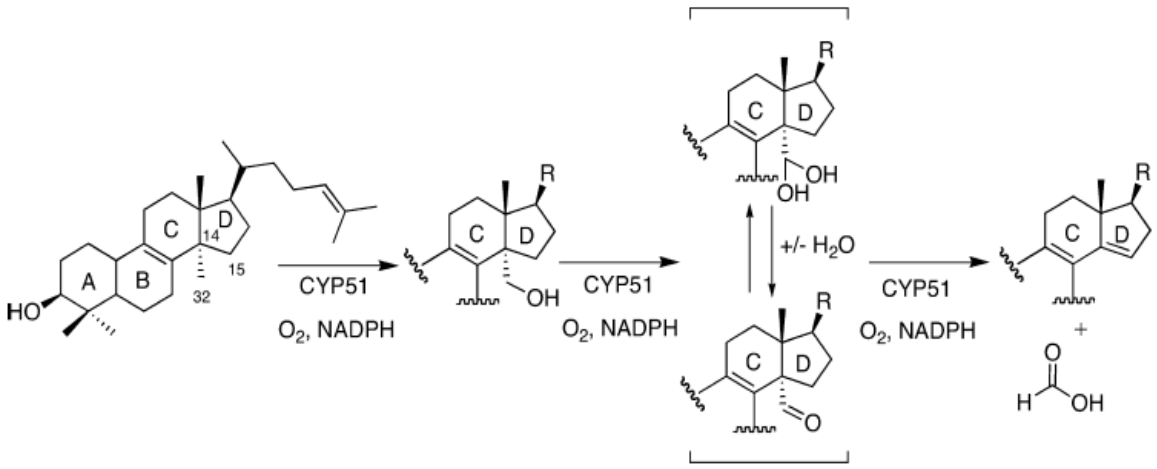

Figure 10: Catalytic intermediates in the CYP51 catalyzed deformylation of lanosterol.

A computational study by Sen and Hackett[47] employed explicit solvent molecular dynamics (MD) simulations and hybrid quantum mechanics/molecular mechanics (QM/MM) techniques to provide mechanistic insight into O_2 activation and characterize reactive oxygen intermediates in Mtb CYP51 catalysis. Simulations of the His259H$^+$ Mtb CYP51 revealed evolution of two networks which could shuttle electrons to the peroxo species in CYP51. The first network involving His-Thr dyad could only support Cmpd 0 formation (Figure 11, A).The second proton transfer network connected the distal O_2 atom to His259H$^+$ and Glu173 via four water molecules. In this configuration of the active site, QM/MM calculations revealed that the peroxo species has an unusual triradicaloid electronic structure, resulting from protonation of Glu173, wherein two either parallel or unparallel electrons are localized on the Fe-O units and the third one on the protonated Glu173 side chain. In spite of being ~9Å away from the active site protonation of Glu173 resulted in polarization of electron density thereby tuning the reactivity of the peroxo intermediate. In such a configuration the barrier for Cmpd 0 and Cmpd I formation is ~2 kcal/mol and ~12 kcal/mol respectively and the products were formed with high exothermicity (Figure 11, B and C). Glu173 is located in the F-helix surrounded by polar residues and an easy access to bulk water making its transient protonation likely. This was an interesting observation since the peroxo intermediate has been implicated in the C-C bond cleavage step catalyzed by CYP51 and other P450 enzymes.[48,49,46,50]The active site structure of CYP51 in such a configuration is depicted in Figure 12. A structural comparison of CYP51 with other X-ray crystal structures of other P450s, CYP101[51], CYP107A1[52], CYP119[53] and CYP51[25] revealed an acidic residue that is conserved in F

helices of many of these enzymes (Figure 13) indicating that such a proton shuttling pathway may exist in other P450s as well.

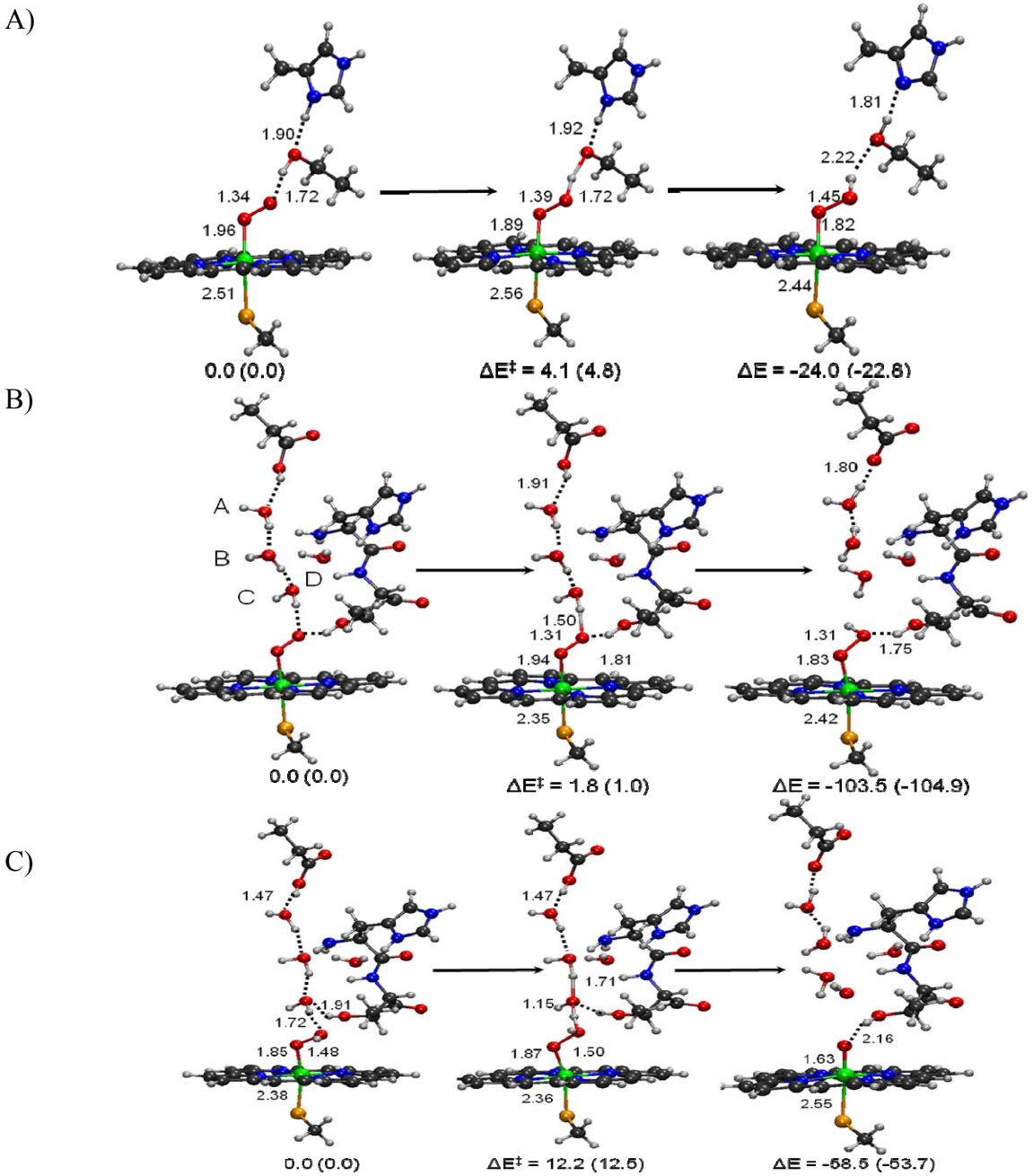

Figure 11: Geometries and energies along the reaction coordinate for A) His259H$^+$-Thr260OH mediated transformation of peroxo to Cmpd 0, B) Glu173-$(H_2O)_4$-mediated transformation of peroxo to Cmpd 0 and C) Glu173-$(H_2O)_4$ mediated transformation of Cmpd 0 to Cmpd 1.

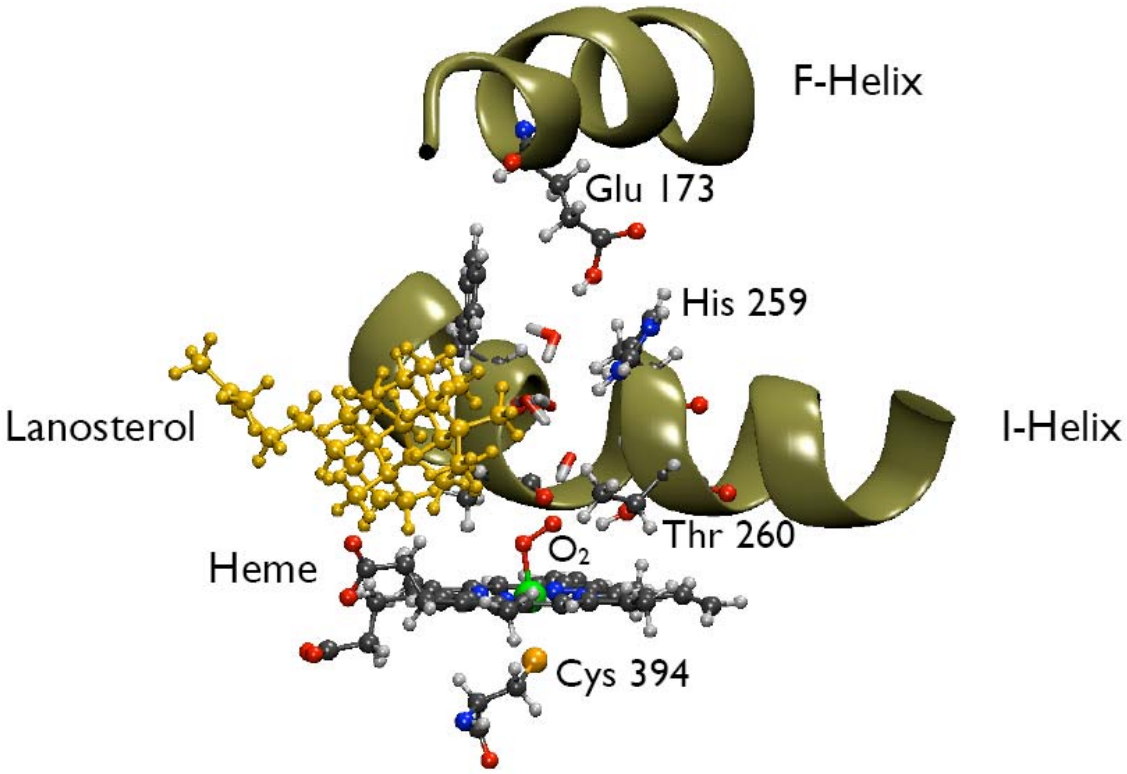

Figure 12: The active site of oxyferrous CYP51. The lanosterol molecule is shown in yellow and the $(H_2O)_4$ network connecting Glu173 to O_2 are shown in a stick representation.

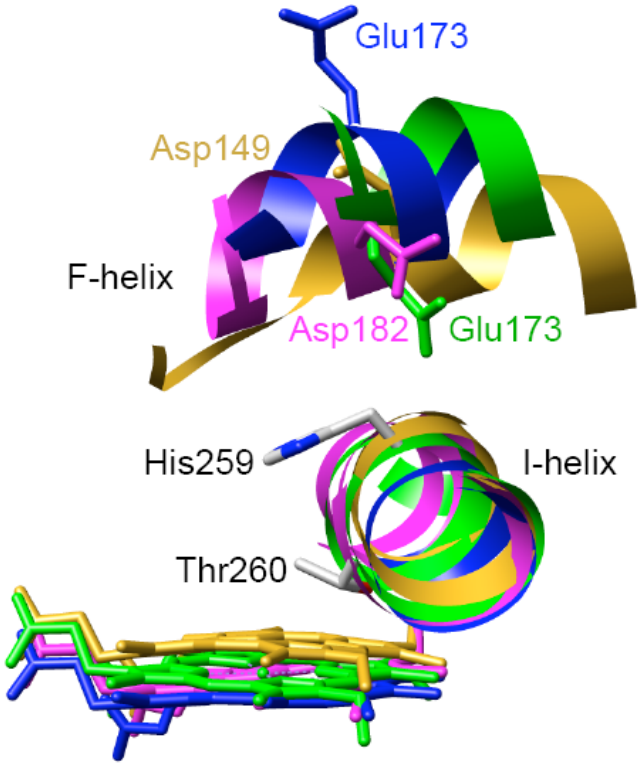

Figure 13: Positions of the I-helices, F-helices and structurally conserved acidic residues of CYP101 (PDB 1DZ8, magenta), CYP119 (PDB 1IO7, yellow) and CYP107A (PDB 1Z8O) as compared to Mtb CYP51 (PDB 1X8V, green).

Based on these computational results Glu173, His259 and Thr260 are thought to participate in the proton shuttle. These residues stabilize the water channel to shuttle protons and orient O_2 for protonation.. Because of their pivotal role in CYP51 catalysis it was decided to mutate these three key residues in CYP51 active site to alanine and characterize the mutants biophysical properties.

2.2 Materials and Methods

CYP51 expression and purification: Initial attempts to clone the CYP51 wild type (CYP51wt) gene in pET 30a gene vector, did not yield much success. The protein expressing plasmid, i.e. CYP51wt gene with a C terminal $(His)_4$ tag in pET17b vector was a kind gift from Dr. Larissa Podust at UCSF.[54] The plasmid was transformed in BL21 (DE3) cells. The transformants were grown at 37°C in LB broth containing 100mM potassium phosphate buffer (pH 7.5), 0.4% v/v glycerol and 100 µg ampicillin. When optical density at 600 nm of the culture attained values between 0.5-0.8, protein synthesis was induced with the addition of 0.2 mM isopropyl-β-D-thiogalactopyranoside (IPTG) (Lab Scientific). 0.5 mM 5-aminolevulinic acid (5-ALA) (Alfa Aesar), a precursor of heme biosynthesis, was added. Cells were grown for 20 hrs at 20°C and harvested by centrifugation at 5000 rpm for 10 mins. The pelleted cells were gently resuspended in buffer A consisting of 500 mM NaCl, 50 mM potassium phosphate (pH 7.5), 0.1mM EDTA and 20% (v/v) glycerol. The cell suspension was lysed in a French press at pressure exceeding 20,000 psi twice. The lysed cells were separated from cell suspension by centrifugation at 20,000 rpm for 20 mins. CYP51 was isolated by using the Ni^{+2}-

nitrilotriacetic acid (Ni-NTA) affinity column (Qiagen). The column was equilibrated with the equilibration buffer consisting of buffer A without 0.1 mM EDTA. The cell lysate was loaded onto the Ni-NTA column and washed with a buffer B consisting of 500 mM NaCl, 50 mM potassium phosphate (pH 7.5), 5 mM imidazole and 20% v/v glycerol, until their absorbance maintained a constant value. The protein was eluted by increasing the imidazole concentration in buffer B to 50 mM. The eluate was dialyzed overnight in 50mM potassium phosphate (pH 7.5) and 20% v/v glycerol. Dialyzed sample was further purified by size exclusion chromatography using HiLoad™ 26/60 Superdex™75 prep grade column (GE healthcare) on a Amersham BioSciences FPLC system. SDS polyacrylamide gel electrophoresis (PAGE) analysis was performed at each stage of the protein purification on a 7% polyacrylamide gel. The protein molecular weight standard was obtained from Biorad. Protein quantitation was done using the Bradford reagent (Biorad).[55]

CYP51 mutagenesis: A standard protocol was followed for mutagenesis of all the CYP51 mutants. The CYP51wt plasmid was used as template DNA. The upstream and downstream primers (Invitrogen, with changed nucleotides in bold/underlined) for Glu173Ala (E173A) are upstream: 5' CT**A**TCACGAGTTGGCGCGCGGCACCGAC 3' and downstream: 5' GT**C**GGTGCCGCGCGCCAACTCGTGATAG 3', His2559Ala (H259A) upstream: 5' G**TT**CGCCGGCCATGCCACCAGCTCGGG 3' and downstream: 5' C**CC**GAGCTGGTGGCATGGCCGGCGAAC 3' and Thr260Ala (T260A) upstream: 5' G**C**CGGCCATCACGCCAGCTCGGGTAC 3' and downstream: 5' G**T**ACCCGAGCTGGCGTGATGGCCGGC 3'. Phusion™ High Fidelity PCR Master Mix

was used for the Polymerase Chain Reaction (PCR) (New England Biolabs) and nuclease-free water was used from Promega. A 50 µL reaction was set up using 0.4 ng of template DNA, and 0.5 µM primer. Amplification conditions were 98°C for 60 s, 25 cycles of 98°C for 10 s, 65-75°C for 25 s and 72°C for 2.00 mins. A final extension was carried out for 72°C for 10 mins. An annealing temperature gradient was done. Following amplification the samples were digested with the enzyme DpnI (New England Biolabs) for one hour. DpnI is a restriction endonuclease which digests methylated plasmids, thus retaining only those plasmids amplified *in vitro*. The samples were then concentrated to 10 µL using a SpeedVac, 5 µL of which was used to analyze by 1% agarose gel electrophoresis in a Biorad gel tank. Agarose gel was prepared by solubilizing 0.5 g of agarose (Biorad) in 50 ml of Tris-Acetate-EDTA (TAE) buffer. Ethidium bromide (Promega) was added to the agarose solution to aid visualization of the amplified bands under UV light. A 1 kb DNA ladder (New England Biolabs) was used as reference. Based on amplification results (Figure 12) the remaining 5 µL solution was transformed in the NovaBlue GigaSingles™ Competent cells (Novagen) using a standard protocol where 5µL of DNA solution was added to 50µL of competent cells and incubated on ice for 5 minutes. Cells were then subjected to a heat shock at 45°C for 45 seconds and placed back on ice for 2 mins. 250 µL of SOC media (Novagen) was added to the cells and they were incubated at 37°C for 1 hour. Following incubation 50 µL of cells were plated on agar plates containing Ampicillin (Fisher) and they were incubated overnight at 37°C. Successful transformants were inoculated and grown overnight in 5 mL of LB broth. Plasmids were extracted using the QIAprep Spin Miniprep Kit (Qiagen) as per manufacturer's recommendations. Plasmids

were sequenced at the VCU DNA core facility using the universal T7P primers. Those showing correct mutations were stored at -20^{o}C.

Expression and purification of CYP51 mutants: Mutants were purified and expressed similarly to the wild type.

Cloning and expression of Mtb Fdx: A ferredoxin (Fdx) is needed to shuttle electrons from a ferredoxin reductase to CYP51 for catalysis to occur. Genomic DNA (gDNA) of the Mtb strain H37Rv was obtained from the TB Research Materials and Vaccine Testing Contract (NO1 AI-75320) at Colorado State University. Ligation independent cloning technique was adapted for cloning of the Mtb Fdx. A pET46-Ek/LIC kit was used from Novagen, which consists of all materials required for the cloning. The pET46-Ek/LIC vector is an open vector having N terminal $(His)_6$ tag and an enterokinase (Ek) protein cleavage site (Figure 14). Primers for Fdx consisted of nucleotides that were complementary to the Fdx gene and certain additional nucleotides were added (underlined and bold) which are required to generate vector compatible overhangs as per specifications mentioned in the accompanying handbook of the kit, upstream-5' **GACGACGACAAG**-ATGGGCTATCGAGAAGCC 3' and down 5' **GAGGAGAAGCCCGG-**TTACTCTCCCGTTTCTCG 3'. Phusion PCR Master Mix was used as a source of DNA polymerase and dNTPs. The PCR reaction was set up using the manufacturer's recommendations.

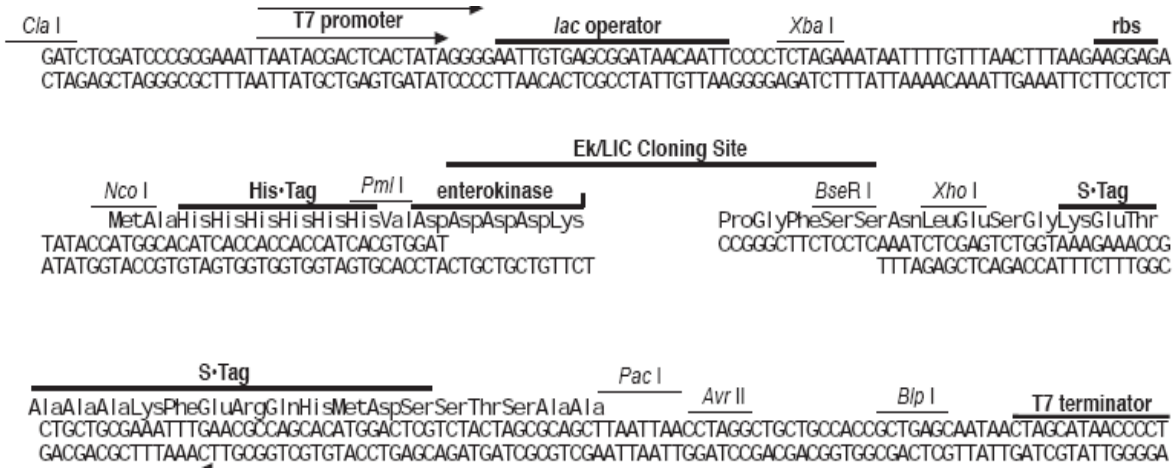

Figure 14: A map of cloning sites in the pET-46 Ek/LIC vector. (from the Novagen pET-46 Ek/LIC handbook).

The PCR product was analyzed on a 1.3% agarose gel with 100 bp ladder (New England Biolabs) as a reference. The amplified band was extracted from the gel using a QIAquick Gel Extraction kit (Qiagen) according to manufacturer recommendations. The amplified DNA was subjected to a T4 Polymerase treatment to generate vector-compatible overhangs. T4 polymerase is an enzyme having dual actions: a 5'- to 3'- polymerase activity and a 3'- to 5'- exonuclease activity. In the presence of all nucleotides the polymerase balances the exonuclease activity by adding nucleotides in the opposite direction. However the system is cleverly unbalanced to generate these overhangs. Because only dATP is present along with the polymerase, the exonuclease activity is continued until the nucleotide T is reached so that the polymerase can add the nucleotide A. The general principal of the working of the ligation independent cloning is depicted in Figure 15. A 20 µL reaction was initiated by adding the T4 DNA polymerase enzyme to the purified PCR product and incubated at 22^{o}C for 30 mins. The enzyme was inactivated by heating at 75^{o}C for 20 mins. The polymerase treated PCR product (4 µL) was annealed to the pET-46 Ek/LIC vector (1.5 µL), by incubating at 22^{o}C for 5 min. At the end of 5 min, 2 µL of 25 mM EDTA was added and the reaction was continued for 5 additional minutes. 2 µL of the annealing reaction was transformed in NovaBlue GigaSingles competent cells and plated on ampicillin containing agar plates. Plates were incubated overnight at 37^{o} C. From the colonies grown overnight, 13 colonies were selected to screen for the presence of insert. They were grown in 5 mL of LB broth and their plasmids were isolated using the Qiagen Miniprep Spin kit. A PCR was done using 1 µL of each of the plasmids as template DNA, maintaining the concentrations of the other components and reaction conditions as

previously described. The PCR products were analyzed on 1.3% agarose gel and those showing appropriate amplification sequenced at the VCU DNA core facility.

The plasmid bearing correct Fdx sequence was expressed just as CYP51wt with a few exceptions. During induction of protein expression, along with 0.2 mM of IPTG, 0.15 mM of $FeCl_3$ was added to the media. For protein purification, buffer A contained 5mM of imidazole instead of 0.1mM of EDTA. After loading, Ni-NTA column was washed with buffer B containing 50 mM of imidazole. To elute the protein imidazole concentration in buffer B was increased to 250mM. Proteins were analyzed on a 4-20% gradient PAGE gel (Thermo Scientific).

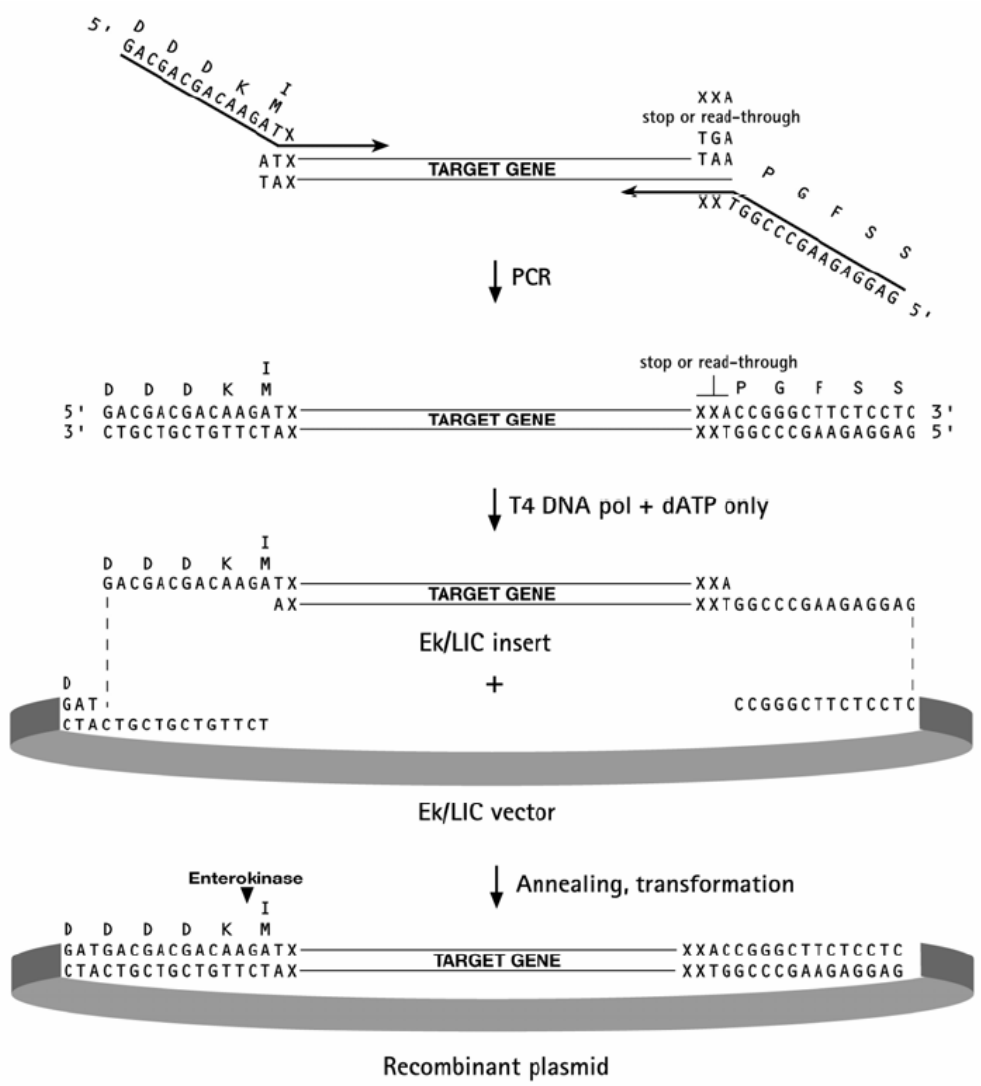

Figure 15: Diagram of the Ek/LIC stategy. (From the Novagen LIC handbook)

Cloning and trial expression of Mtb CYP132: A protein BLAST analysis of Mtb CYP132 revealed that it was similar to many of the human CYP4V family of P450s, which are putative fatty acid oxidizing P450s.[56] This was an interesting observation given the lipid rich nature of the mycobacterial cell wall. We cloned and tried to express the CYP132 protein by the LIC strategy. Primers having the sequence upstream 5' **GACGACGACAAG**ATGGCCACCA-CCACCCAGCGGCCCCTGAAG 3' and downstream 5' **GAGGAGAAGCCCGG**TTATCGCCTCCTCCCGATGACGTGT-ACTCCGTG 3' (Invitrogen) were used to amplify the gene for insertion into pET 46-Ek/LIC vector. CYP132 cloning methodology was similar to that of Fdx with few exceptions in the PCR amplification conditions. At the time of induction of protein formation 0.5mM of δ-amino levulinic acid was added to the media. Expression of CYP132 proved to be cumbersome because of inability of the protein to express in a soluble form. A variety of different conditions were tried for protein expression. Protein purification protocol remained similar to that to Fdx.

Spectral analysis of CYP51wt, CYP51 mutants and Fdx: The oxidized and reduced forms of P450 proteins were analyzed in 1.6 mL quartz cuvette on a Shimadzu UV double beam spectrophotometer, as per standard protocols.[57] The carbonmonoxy (CO) difference spectra were determined as per methods described by Omura and Sato.[58] Binding assays were performed in 1.6 mL quartz cuvette using 25 μM P450 concentration in the dialysis buffer. Standard compounds dissolved in ethanol (11.5 mM.for clotrimazole (Sigma) and 12mM for estradiol) were added to the protein solution in 2 μL aliquots. Same volume of ethanol was added to the reference cell and the difference spectra were recorded in the

range of 350 nm-550 nm. Binding constants were obtained by plotting a double reciprocal plot of $\frac{1}{\Delta A_{max}}$ against $1/[S]$, using equation $\frac{1}{\Delta A_{max}} = \left(\frac{K_S}{\Delta A_{max}}\right)\frac{1}{[S]} + \frac{1}{A_{max}}$, where $\left(\frac{K_S}{\Delta A_{max}}\right)$ is slope of the line. For Fdx, just the oxidized and reduced spectra were recorded.

Reconstitution of FnR/Fdx/CYP51 electron transport: To verify whether the electron transport chain was functional in supplying electrons to CYP51 from NADPH via Fdx and spinach ferredoxin reductase (FnR), ferrous-CO spectra were obtained. In order to obtain a ferrous-CO spectrum, the P450 sample is reduced in both the sample and reference cuvette using few grains of sodium hydrosulfite and CO is bubbled in the sample cuvette. Ligation of CO to the reduced P450 produces strong absorption maxima at 450 nm. The electron transport chain experiment is similar to the ferrous-CO experiment except in this case the reduction is performed by FnR and Fdx with NADPH as the electron source (Figure16). 5 mg CYP51wt, 0.269 mg Fdx, 0.2 Units of FnR were assembled in a 1.6 mL quartz cuvette. NADPH was added to both the sample and reference cuvettes and a baseline was recorded. Then CO was bubbled in sample cuvette and a difference spectrum was recorded. The working of the electron transport chain was investigated in mutants in a similar manner.

CYP51wt catalytic activity assay: The Mtb CYP51 enzyme is more plant like than animal like, hence obtisifoliol which has a 98% turnover rate is a better substrate for the catalytic activity than lanosterol, the turnover rate of which is just 1%. On the other hand, dihydrolanosterol (DHL) in which the 24,25 double bond is absent, is a better substrate for this enzyme with a turnover rate of about 20%.[38] Due to commercial unavailability of DHL it was made from lanosterol by a one step hydrogenation. (Figure 17) The starting material,

Lanosterol (Steraloids, Inc) was assessed for purity by TLC, using a solvent system consisting of 90:10 hexane:ethylacetate. It was purified on a silica column using the same solvent system and samples were analyzed using ^{1}H-NMR. The reduction reaction was carried out in a hydrogenation apparatus using 0.1M of the starting material and 10% PdC in ethanol

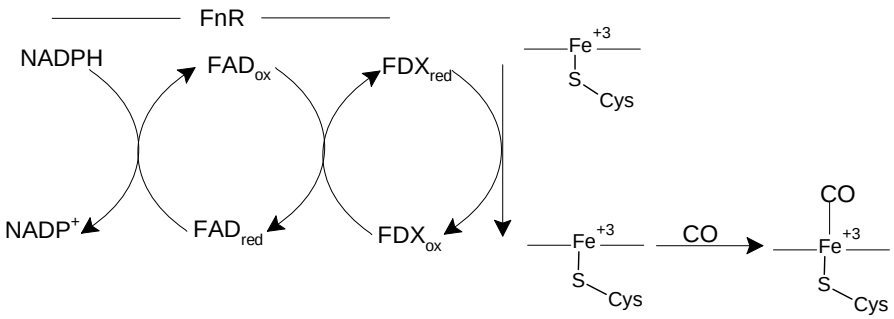

Figure 16: Electron transport chain in CYP51. Electrons are transferred from NADPH to CYP51 via Fdx using FnR. Reduced P450 binds to CO resulting in Soret band at 450 nm (inset).

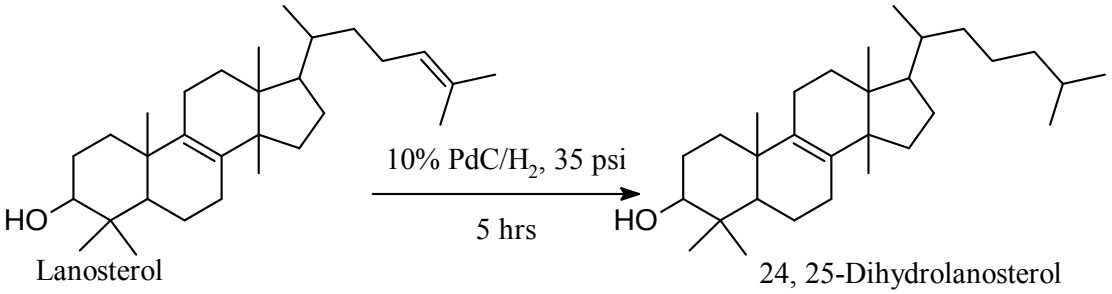

Figure 17: One step reduction of lanosterol to dihydrolanosterol.

The pressure was set at 35psi and reaction was carried out for 5 hours. After 5 hours the reaction was filtered using celite and methanol. The product was dried by evaporating the solvent on vacuum.

To solubilize DHL, 0.1mM of DHL was dissolved in 1 ml of methanol and added to 16 mg of Triton WR1339 (Sigma) dissolved in 1 ml of methanol. Methanol was evaporated using vacuum and the residue was resuspended in equal volume of water. For the assay 50 mM potassium phosphate buffer (pH 7.5), 0.5µM of Cyp51wt, 1 µM of Fdx and 0.1 unit of Fnr and 0.1 mM of DHL were incubated on ice for 10 mins. Reaction was initiated by adding 0.4 mM of NADPH (Sigma) and carried out for 6 hours at 30^{o}C. Product was extracted using 5 vol of ethylacetate, which was evaporated to complete dryness in a GeneVac centrifugal evaporator. The residue was resuspended in 0.5 ml of methanol and injected into Shimadzu LC. The run was set for 40 mins and the solvent sytem was a linear gradient of methanol and methanol:water:acetonitrile (45:10:45) over 30 mins and 100% methanol for 10 mins.

2.3 Results and Discussion:

Mtb CYP51wt: The CYP51wt gave an excellent expression (5mg/L culture) of protein in the BL21 (DE3) strain of *E.coli*. A single band at 50 kDa was observed on the SDS-PAGE gel, (Figure 18, A). The ferrous-CO spectrum shows a major peak at 450 nm and a smaller peak at 420 nm. However, unlike in typical P450s the peak at 450 nm decays to a form of the enzyme absorbing at 420 nm.(Figure 18,B-2). This can be attributed to the protonation of the cysteine thiolate ligand. The oxidized spectrum of purified CYP51, showed a Soret peak at 420nm and the charge transfer bands 573 nm (α) and 541 nm (β). Reduction by sodium hydrosulfite (Sigma) resulted in a Soret peak at 423 nm (Figure 18, B-1).

A)

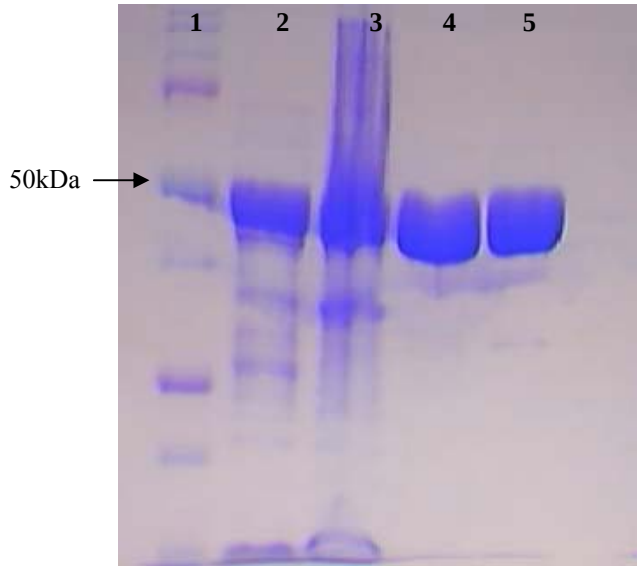

Ln1 Ladder

Ln2 Cell lysate

Ln3 Pellet

Ln4 Eluted protein

Ln5 Dialyzed protein

B)

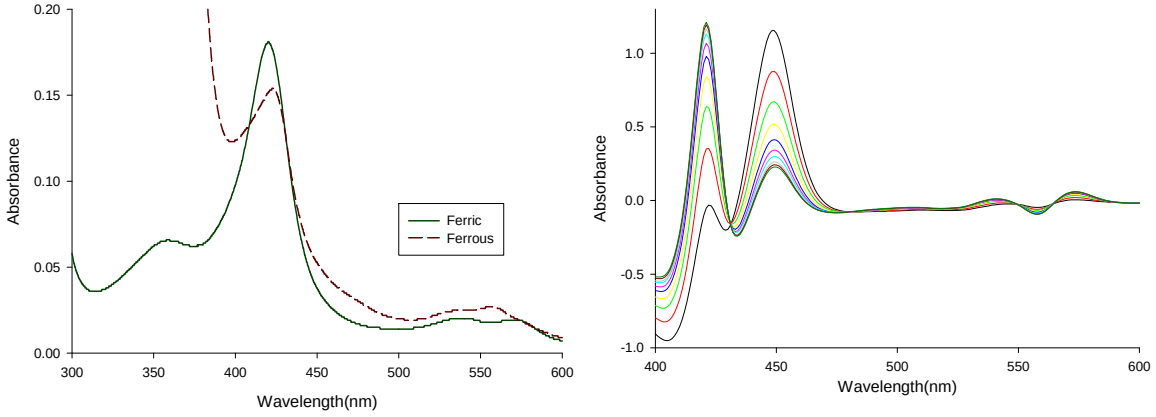

Figure 18: Analysis of CYP51wt A) SDS-PAGE gel showing band near 50 kDa. B) UV-vis spectra of the ferric and ferrous oxidation states of CYP51. C) UV-vis spectra showing a collapse of the P450 complex of CYP51 to the P420 complex.

Type I substrate binding in P450s causes a change in the spin state from high spin to low spin due to the loss of water as the sixth ligand and the resulting spin shift causes a peak at 388 nm and a trough at 423 nm in CYP51 (Figure 19, A). The azoles are known inhibitors of 14α-demethylase enzymes [59, 60] and these molecules produce a type II spectrum, resulting from the direct coordination of the azole to the heme as the sixth ligand. The type II spectrum is characterized by a peak at 432 nm and a trough at 411 nm. (Figure 19, B). A third type of ligand like *n*-butanol produce a reverse type I spectra The binding mode of type I, II and reverse type I and the resulting difference spectra are summarized in Figure 19. In both type I and type II ligand spectra, the spectral shift is proportional to the P450-substrate complex. The binding constants of CYP51wt for estradiol and clotrimazole are summarized in Table 2.

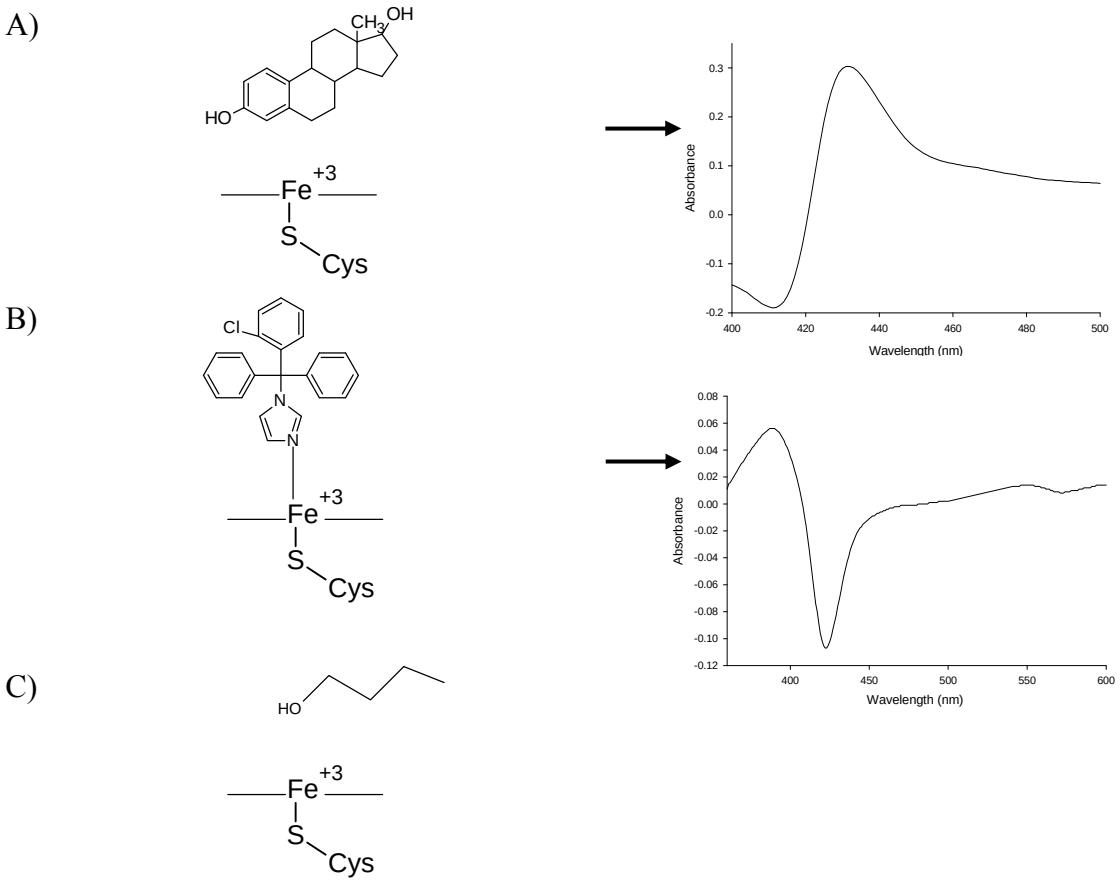

Figure 19: Different type of ligands for P450s A) type I-estradiol B) type II-clotrimazole and C) reverse type I-*n*-butanol. Difference spectra results from the subtraction of the water coordinated species from the ligand bound species.

A)

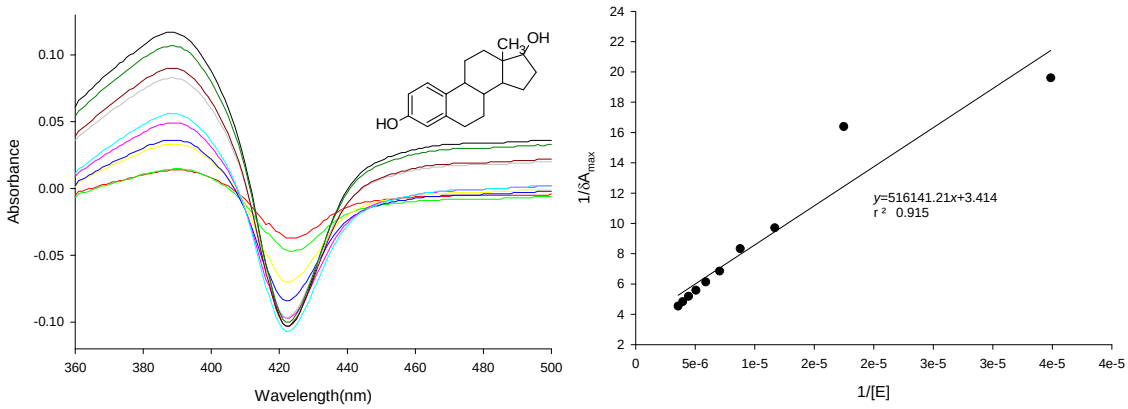

B)

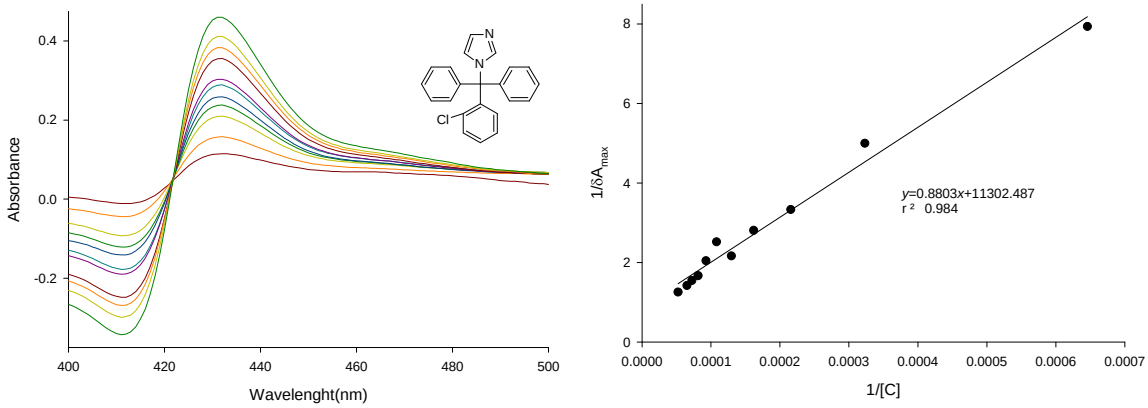

Figure 20: Difference spectra arising from titration of CYP51wt with, (A) 17β-estradiol and (B) Clotrimazole. Linear fit to $\frac{1}{\Delta A_{max}} = \left(\frac{K_s}{\Delta A_{max}}\right)\frac{1}{[S]} + \frac{1}{A_{max}}$

Mtb CYP51 mutants E173A, H259A and T260A: PCR showed good amplification of the target plasmid between 4-5kb (Figure 21, A) SDS-PAGE analysis showed a single band around the expected 50kDa range (Figure 21, B). Spectral analysis of mutants in described in Figure 22 and the peaks observed in the spectra of mutants are summarized as follows in Table 3. While H259A and E173A showed comparable spectra to that of the wild type, T260A mutant had a few distinct spectral properties. The ferrous species showed the presence of an extra peak at around 476 nm and the ferric spectra was quite diffused compared to the ferric species of other mutants and the wild type. The P450 species in the T260A ferrous-CO difference spectra was unstable and it immediately collapsed to the P420 species.

Table 2: UV-vis spectral characteristics of CYP51 mutants.

Mutant	Ferric	Ferrous	Ferrous-CO, α, β.
Glu173A	419.2 nm	423 nm	450.8 nm, 574 nm, 541 nm.
H259A	418.4 nm	425.6 nm	449.2 nm, 574 nm, 542 nm.
T260A	417.8 nm	425.2 nm	449.6 nm, 476 nm, 575 nm, 541 nm.

A)

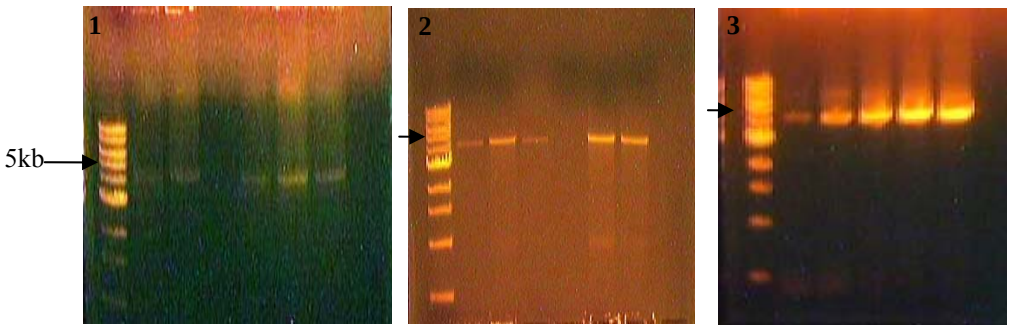

B)

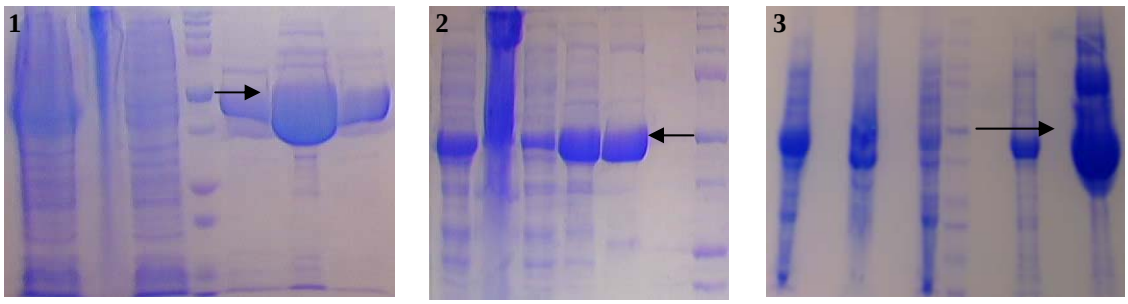

Figure 21: Agarose electrophoresis and SDS-PAGE analysis of mutants. A) Agarose gels showing PCR amplification of the CYP51 mutants 1) E173A, 2) H259A and 3) T260A below 5kb as pointed by the arrow. B) Corresponding SDS-PAGE of the mutants, the arrow points from the 50kDa band of the marker to the eluted fraction of the protein.

A)

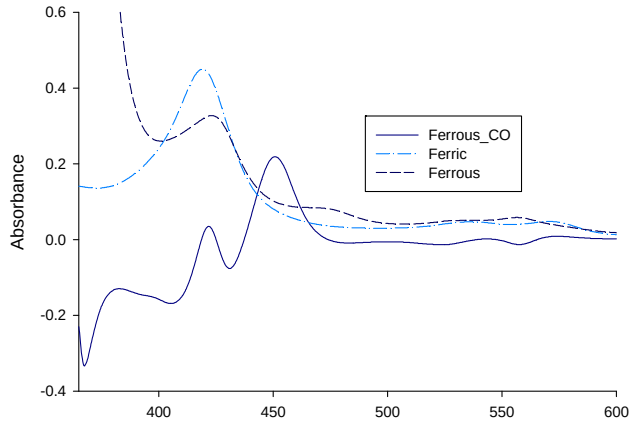

B)

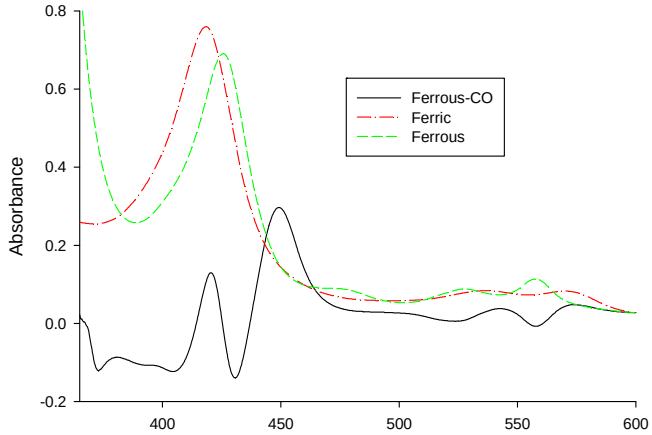

C)

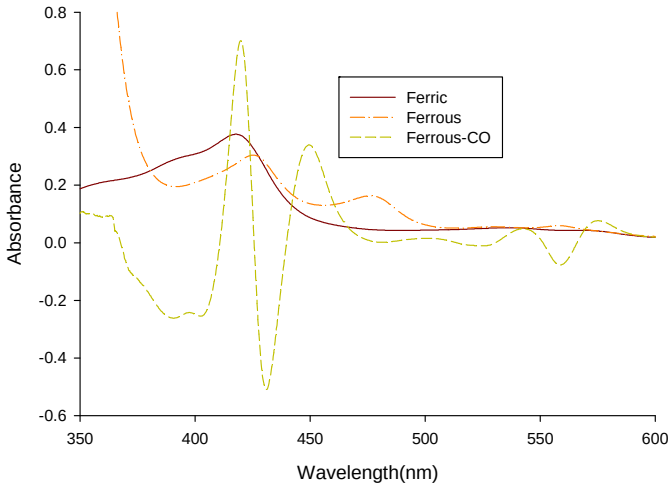

Figure 22: Ferric, Ferrous and Ferrous-CO spectra of CYP51 mutants. A) E173A, B) H259A and C) T260A

Binding studies in the mutants using type I and type II ligand yielded values quite different from those for wild type, especially for the type I ligand, estradiol. Saturation was achieved with low concentrations of imidazole in the titration experiments. The difference spectra and linear plots are shown in Figure 23 for estradiol and Figure 24 for clotrimazole. Dissociation constants are summarized in Table 2. Binding constants of the mutants for estradiol deviated from those for CYP51wt, which can be assumed to be attributed to change in active site architecture. Binding constants for the E173A mutant showed significant differences in both the type I and II ligand as compared to the CYP51wt. Among these mutants, binding spectra of T260A showed the most distinct spectral properties. In type I difference spectra it showed a distinct red shift with a peak at 415nm and a trough at 380nm. This is quite similar to the difference spectra produced by the reverse type I ligand, for example *n*-butanol and phenacetin.[15] This may be attributed to the unavailability of a hydrogen bond donor at the active site due to the mutation in the Thr residue.

Table 3: Dissociation constants for CYP51wt and mutants:

CYP51	Estradiol	Clotrimazole
CYP51wt	151.1 µM	12.8 µM
E173A	4.9 µM	27.6 µM
H259A	18.6 µM	11.0 µM
T260A	34.2 µM	8.5 µM

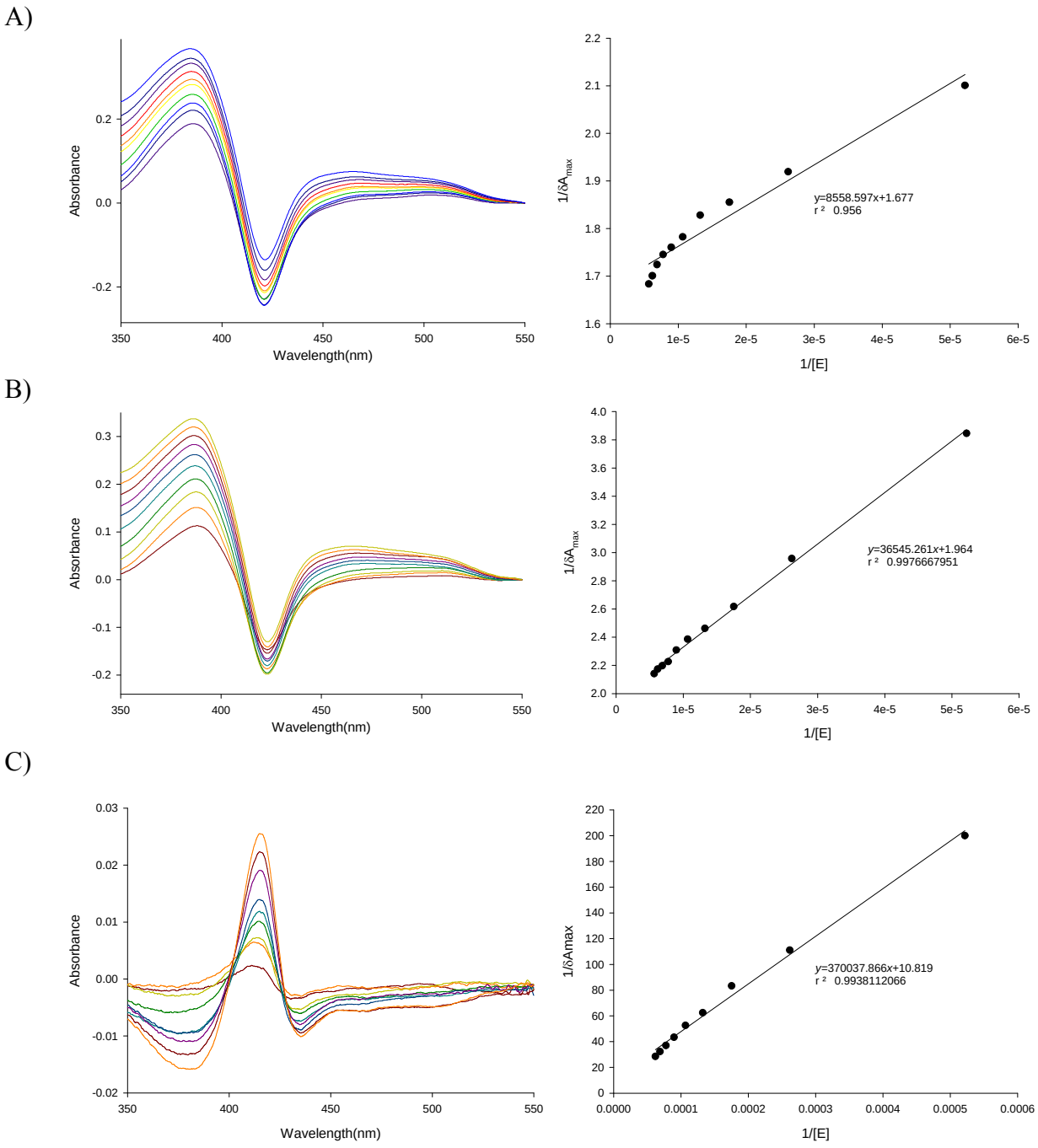

Figure 23: Estradiol binding spectra for CYP51 mutants A) E173A, B) H259A and C) T260A. The graph on left is the difference binding spectra and on right is the linear plot.

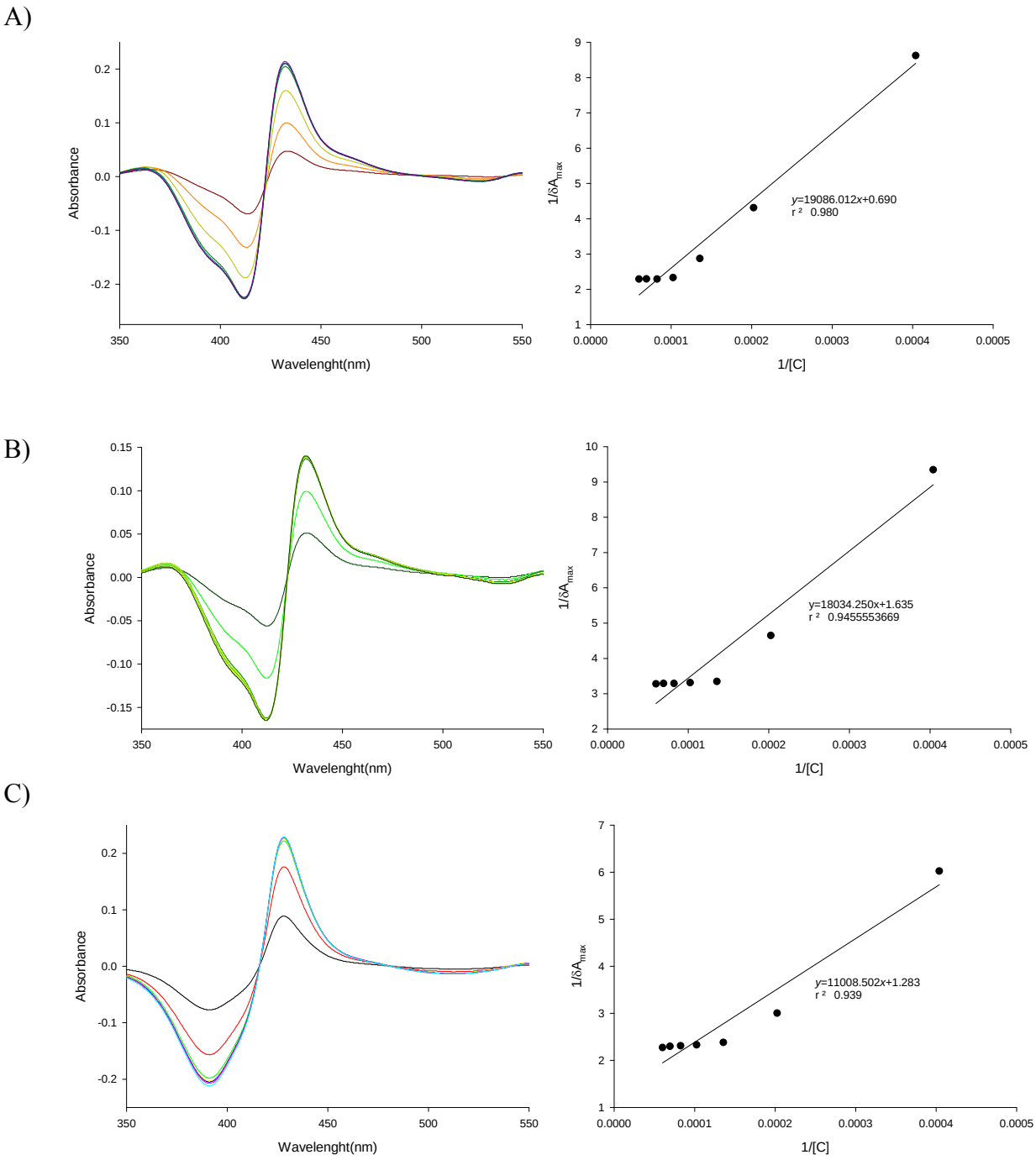

Figure 24: Clotrimazole binding spectra for CYP51 mutants A) E173A, B) H259A and C) T260A. The graph on left is the difference binding spectra and on right is the linear plot.

Mtb Fdx: PCR of the Mtb Fdx gene showed amplification around 200 bp which is consistent with the gene length of 207 bp (Figure 25, A-1). Protein expression of Fdx was good with a yield of 8 mg/L of culture. SDS PAGE analysis of the protein showed a band below the 10 kDa mark (Figure 25, A-2). The spectrum of pure Fdx protein showed a peak at 411 nm and absorption shoulders at 450 nm and 550 nm. The reduced protein spectrum shows a peak at 311nm (Figure 25, B). All the data was in accordance with published literature for similar ferredoxin.[61]

Mtb CYP132: PCR of the CYP132 gene showed amplification below 1.5kb mark of the DNA ladder consistent with the size of the gene (1386bp) (Figure26, A). Expression of a soluble CYP132 protein was unsuccessful. Various temperatures and cells were used to express CYP132. However protein invariably ended up in the inclusion bodies as indicated by SDS gel analysis comparing with protein ladder at 50kDa. (Figure 26, B).

Electron transport chain investigation: Electron transport to CYP51wt was investigated using ferrous-CO difference spectra experiment. Just as seen for reduction with sodium hydrosulfite, at 5 min intervals after reduction a slight peak at 450 nm was seen. Over next 20 mins the peak at 420 nm increased in amplitude (Figure 27). This is an indication of shuttling of electrons from NADPH to CYP51wt, reducing the P450 and allowing it to coordinate to CO and proves that Fdx is functional. The spectra for the mutants were collected at 3 minute interval and it was noticed that for the T260A and H259A, the rate of electron shuttling is an order of magnitude slower than that for E173A.

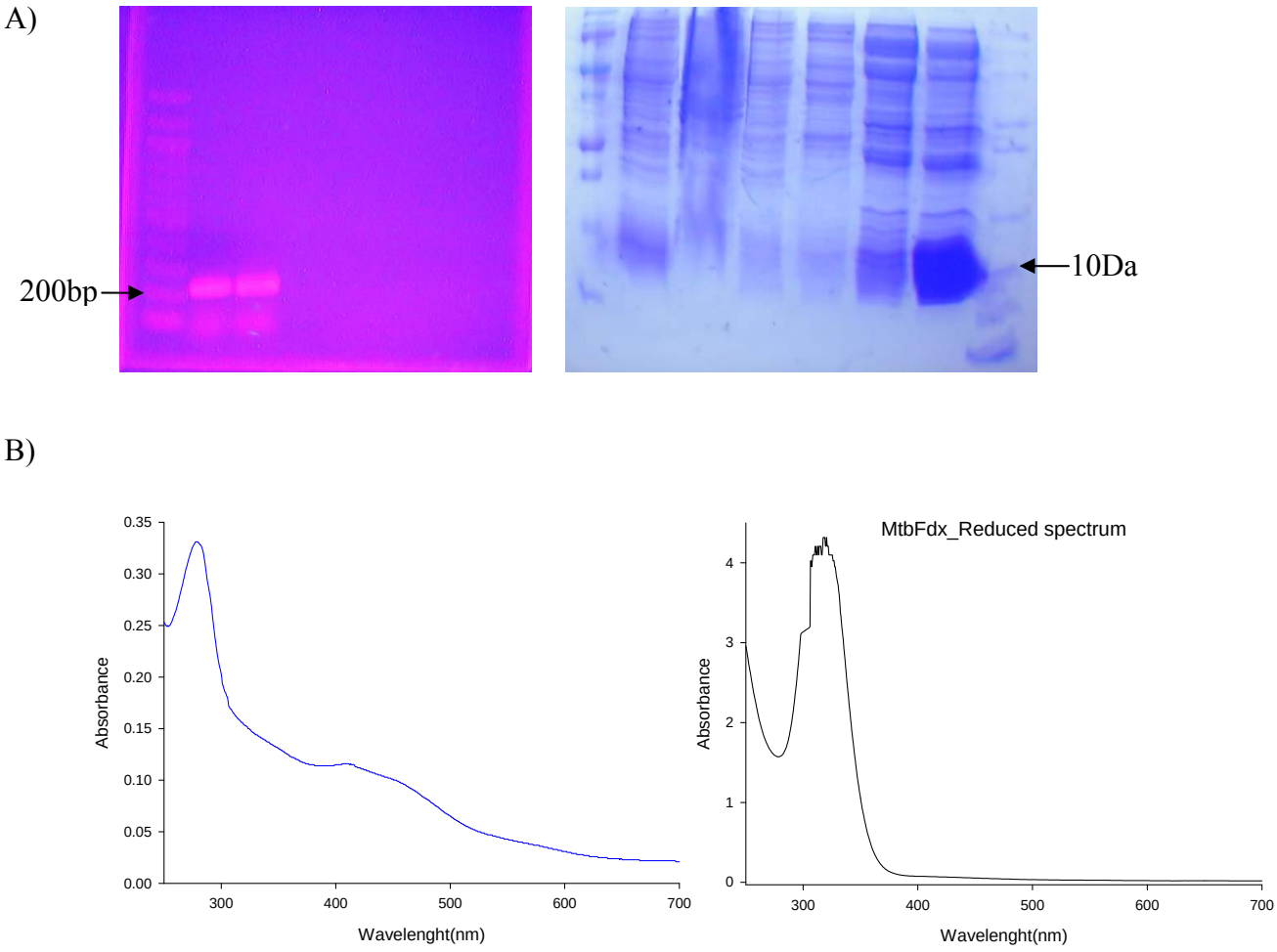

Figure 25: Analysis of Mtb Fdx. A) (left) PCR amplification of the Mtb Fdx gene showing amplification in the 200bp region. (right) SDS-PAGE analysis of Mtb Fdx showing a band near 10Da mark of the protein ladder. B) (left) Oxidized and (right) reduced spectra of Mtb Fdx.

A)

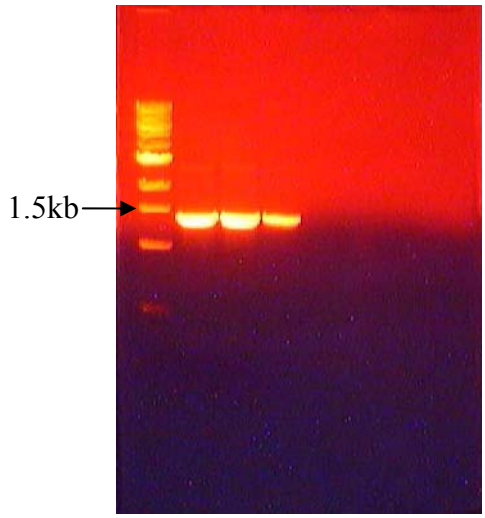

B)

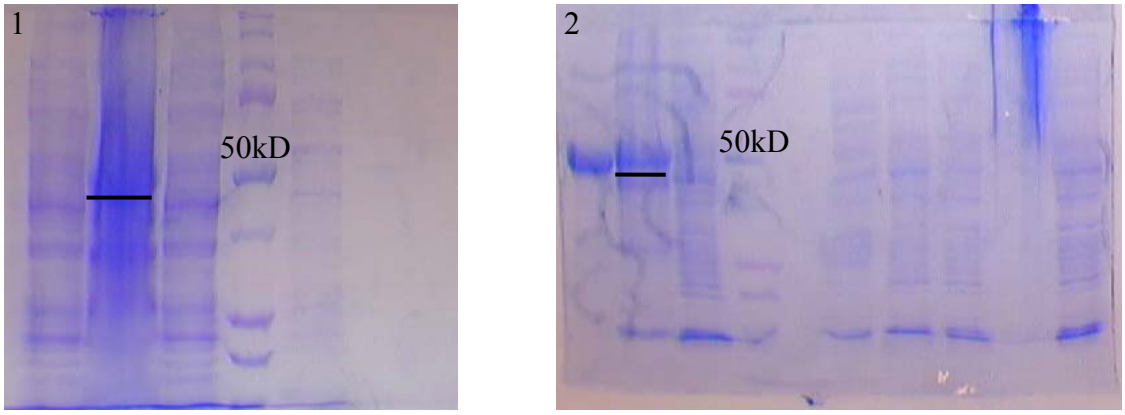

Figure 26: Agarose gel electrophoresis and SDS-PAGE analysis of Mtb CYP132 A) PCR amplification of CYP132. B) SDS PAGE analysis of CYP132, 1) Protein expressed at in BL21 cells at 25°C. 2) Protein expressed in Origami DE-3 cells at 20°C. IPTG concentration was maintained low (0.1-0.2mM) in both the conditions.

CYP51wt catalytic activity assay: In the one step hydrogenation step to make DHL the purified starting material had R_f value of 0.48, its ^{1}H-NMR spectrum is shown in Figure 28 A. Completion of the reaction was checked on UV. Since the end product was UV-invisible it was analyzed by ^{1}H-NMR (Figure 28 B). Repeated attempts to perform catalytic activity didn't yield much success mainly due to failed attempts to solubilize insolubility of DHL in water. In all experiments DHL couldn't be dissolved in the solution, which may have prevented it from being accessible to the enzyme.

A)

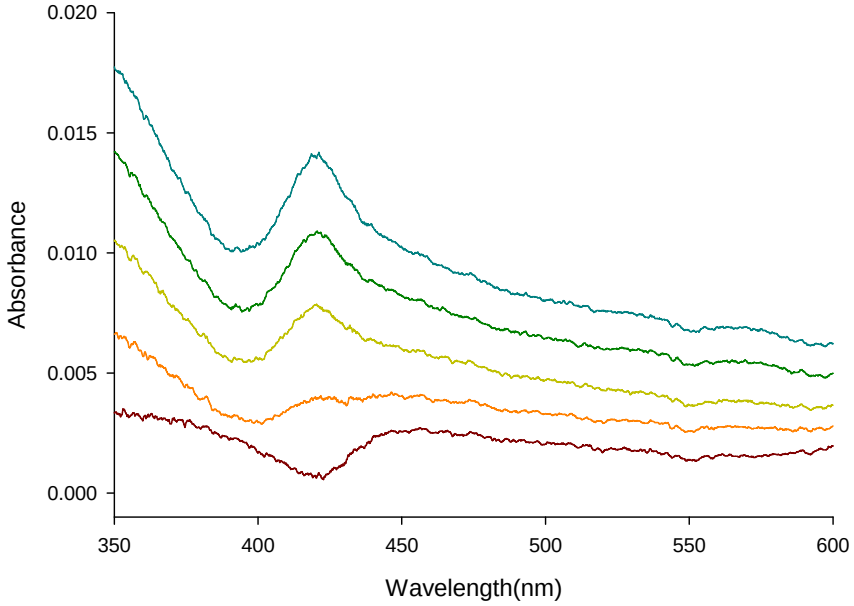

B)

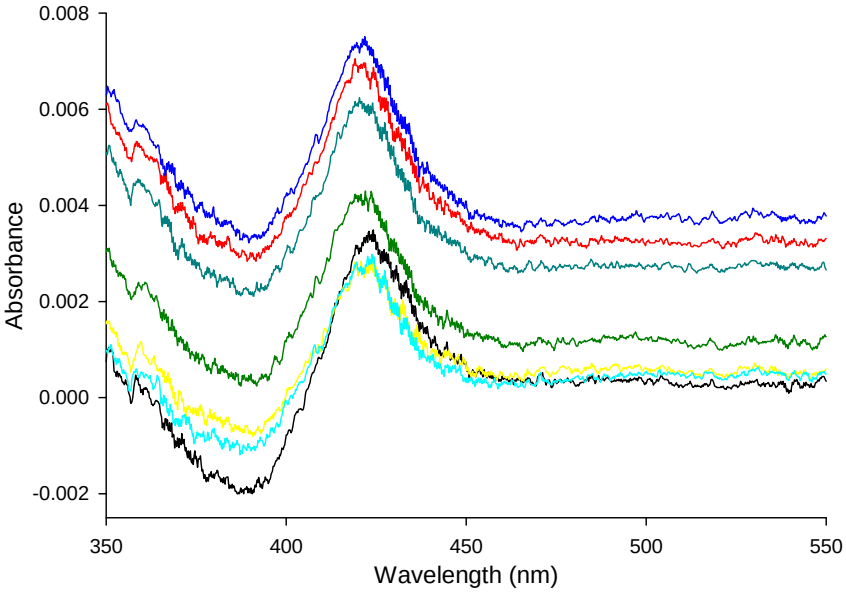

C)

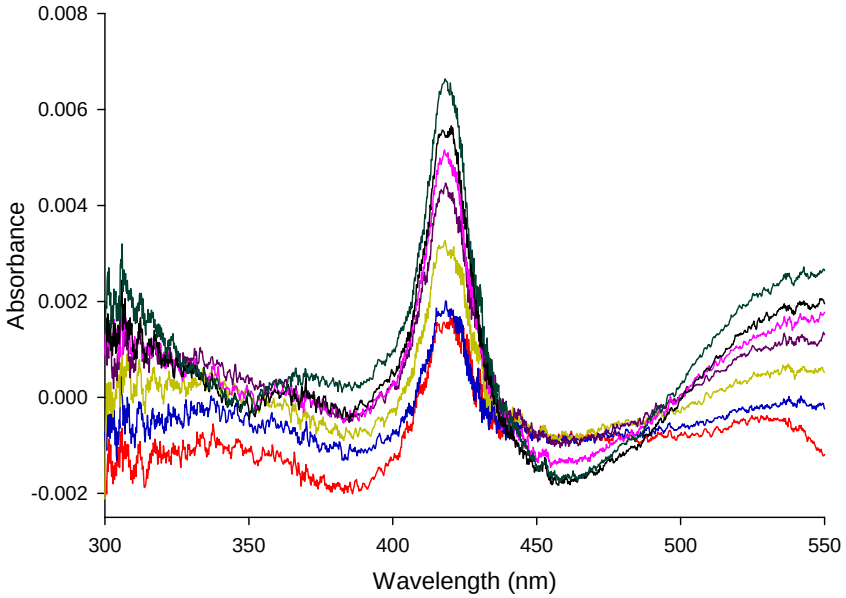

D)

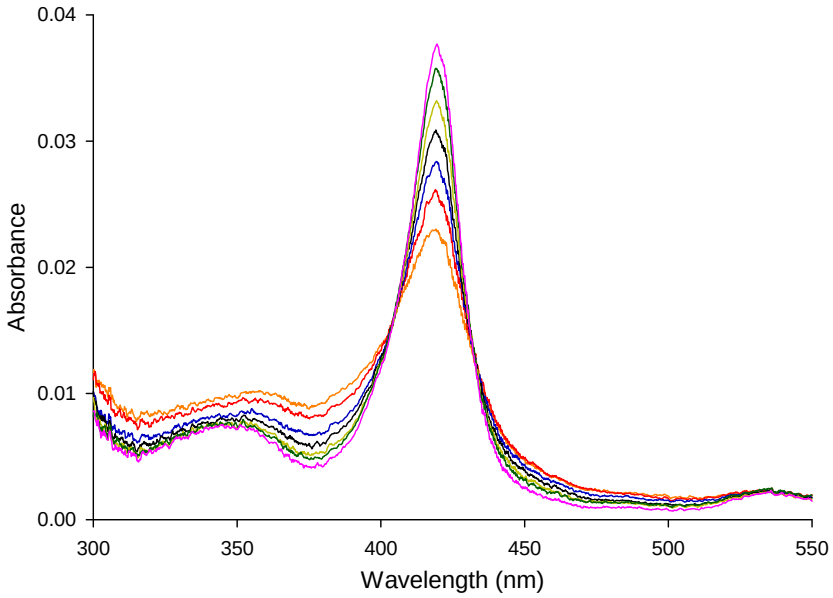

Figure 27: Difference spectra supporting electron transport from NADPH to CYP51, gradual increase in P420 peak indicating reduced P450 coordinating to CO, A)CYP51wt, B)T260A, C) H259A and D) E173A.

A)

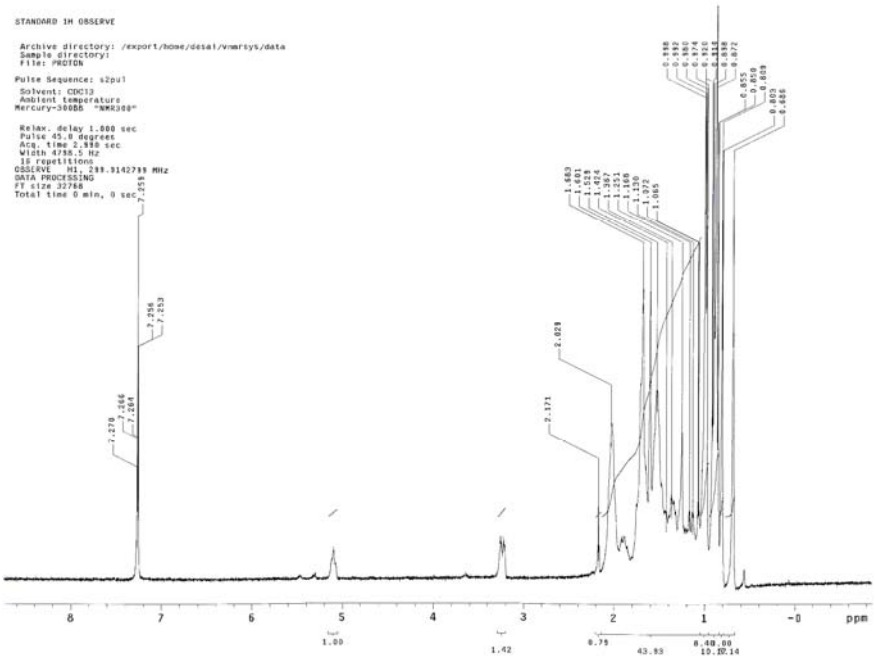

B)

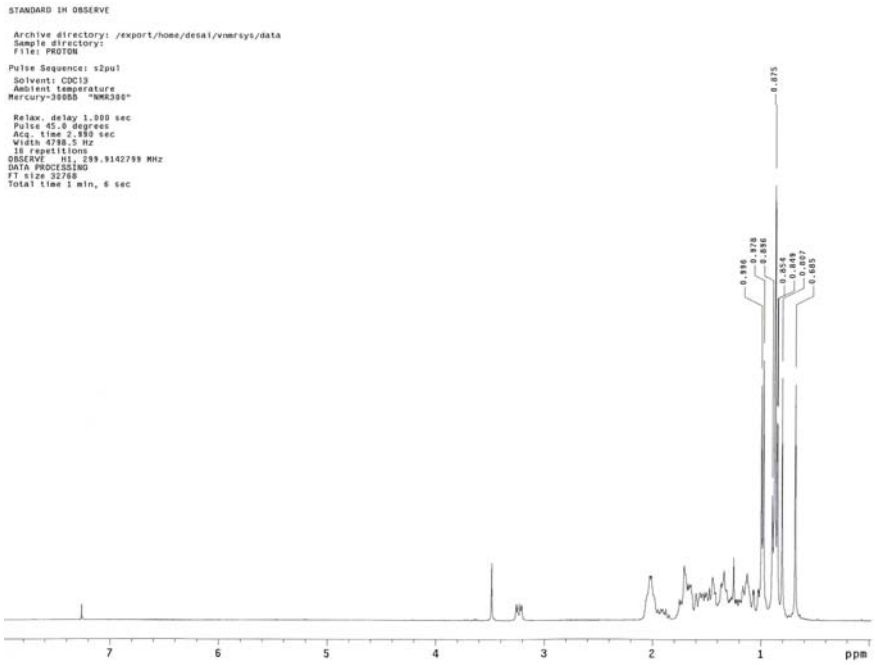

Figure 28: ^{1}H-NMR profiles of A) lanosterol and B) DHL.

CHAPTER 3: Resonanace Raman spectroscopy of CYP51wt and T260A

3.1 Introduction:

Raman effect is an inelastic scattering phenomenon of light.[62] When a light wave, considered as an oscillating dipole, interacts with a molecule some part of the light is absorbed by it and causes polarization. This induces an instantaneous dipole moment in the molecule. The induced dipole μ_{ind}, depends on the applied field E and ease with which the electrons in a molecule are distorted,

$$\mu_{ind} = \alpha E$$

where α is the polarizability of the molecule.[63] When a molecule is excited from ground vibrational level and returns to the same state the frequency of scattered light is identical to incident frequency giving rise to Rayleigh scattering. However, if the excited molecule returns back to a higher (Stokes) or a lower vibrational state (Anti- Stokes) than what it started in, it results in Raman scattering (Figure 29).

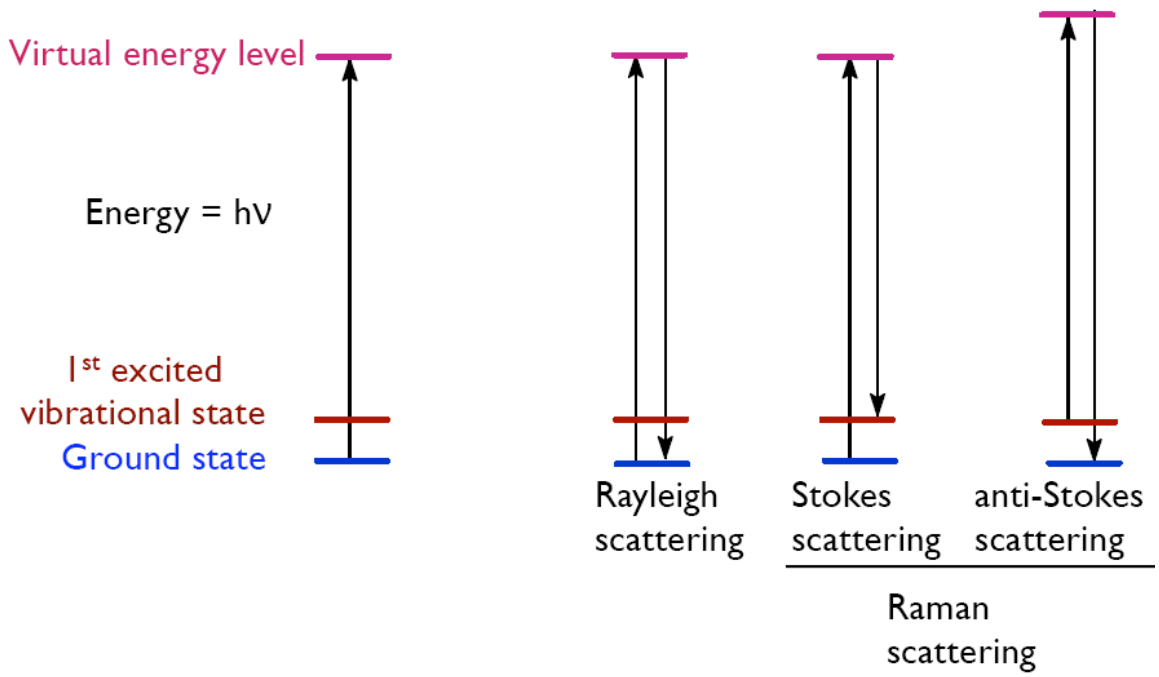

Figure 29: Diagrammatic description of Raman scattering.

When an intense radiation is used to excite a chromophore, light absorbed in the molecule causes strong fluorescence or photodecomposition of the molecule. This hinders Raman detection. However if the sample is excited using a laser at a frequency closer to that of the chromophore, it will give more efficient scattering and more information can be obtained about the electronic and vibrational properties of the sample. This forms the underlying basis of resonance Raman technique. To obtain resonance Raman spectra a laser beam having excitation frequency closer to that of the electronic transition of the molecule under study is chosen. The intensity of Raman scattering is defined by

$$I = K l \alpha^2 \omega^4$$

where, K consists of constants such as speed of light, l is the laser power, ω is the frequency of incident radiation and α is the polarizability of electrons in the molecule.[63] The resonant condition is met when the energy of exciting light matches the energy difference between the lowest vibrational state of the ground electronic state and the resonant vibronic state. Under this condition polarizability increases giving intense Raman scattering. Resonance Raman spectroscopy differs from Raman spectroscopy in the nature of interactions of vibronic states. Under resonating conditions most of the interaction is with one vibronic state, so the scattering is wholly dependent on properties of that state.

In recent years resonance Raman spectroscopy has become a useful tool technique to study heme containing enzymes.[64] The resonance Raman scattering of heme enzymes is attributed to an interaction with π-π^* transitions from the porphyrin ring of the heme group. Resulting vibrations from resonance Raman scattering can be assigned to certain structural properties. Vibrations shown in Figure 30 are markers for the oxidation and spin

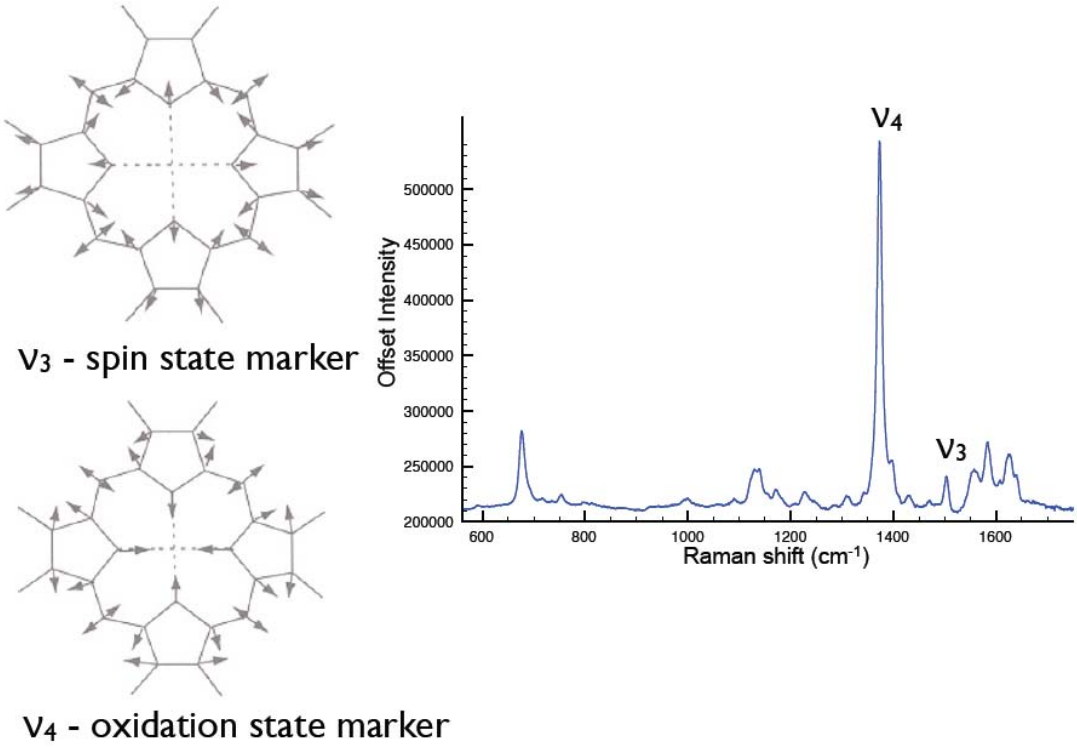

Figure 30: Typical vibrations in heme and their corresponding markers in resonance Raman spectra. [63]

state of the Fe ion in prophyrin.[63] The υ_4 band at ~1373nm is the strongest. It results from the oxidation state of the Fe and major contribution to the υ_4 band is symmetric inward or outward in phase vibrations of the N atoms pyrrole rings coordinated to the central Fe atom. This movement alters the size of the cavity in which the Fe ion sits. The size of the Fe changes with oxidation state making υ_4 band a marker of oxidation state of the central ion. The υ_3 and υ_{10} are markers for the spin state of the Fe ion. Both these vibrations cause significant movement of the inner atoms of the porphyrin. Other vibrations result from the in-plane and out-of-plane movements of porphyrin ring. Since P450s have intense Soret absorption at 410 – 450nm, excitation of frequency close to the Soret absorption band produces Raman scattering enhancing the contributions from totally symmetric A_{1g} modes of vibrations and enabling elucidation of the heme environment.

Resonance Raman spectra were collected for CYP51 and T260A mutant of CYP51 to probe the impact of mutation on the heme environment.

3.2: Materials and Methods:

Resonance Raman spectra was obtained using 5 mw or less of 406.7 nm radiation of the sample,~0.1 mM of CYP51 and T260A The laser used was a Coherent Sabre DBW krypton ion laser and the spectra was acquired using a Princeton Instruments $N_2(l)$ cooled 1340 x 400 CCD detector. The spectrometer was a Spex model 1870 0.5 m spectrometer fitted with a 1200 or 1800 line/mm holographic grating (Jobin-Yvon). Sample exposure times were 2 to 4 minutes. The samples were contained in a quartz Raman spinning cell that was stoppered with a septum. The spinning cell apparatus was from Spex. KCN and

NO were used to record spectra with diatomic ligands. Sodium hydrosulfite was used to reduce samples. A general setup of the Raman spectrometer is shown in Figure 31.

3.3: Results and Discussion:

The resonance Raman spectra for the CYP51wt and T260A mutants were recorded in the ferric, ferrous, NO-ligated and CN^- ligated forms. The wild type and the mutant forms have been compared and shown in Figure 32A-ferric CYP51wt and ferric CYP51T260A, 32B-ferrous CYP51wt and ferrous CYP51T260A, Figure 33A- ferric CYP51wt_CN and ferric CYP51T260A_CN, 33B-ferrous CYP51wt_CN and ferrous CYP51T260A_CN and Figure 34A- ferric CYP51wt_NO and ferric CYP51T260A_NO, 34B-ferrous CYP51wt_NO and ferrous CYP51T260A_NO. The υ_3 band, which is a marker of the spin state, of ferric T260 mutant shows a distinct split as compared to the υ_3 of ferric wild type enzyme indicating the presence of an admixture of two spin states. This suggests that the Thr260 may be involved in hydrogen bonding to the water molecule in order to hold it in place over the heme enzyme, thus helping heme to maintain its low spin hexa coordinate form.

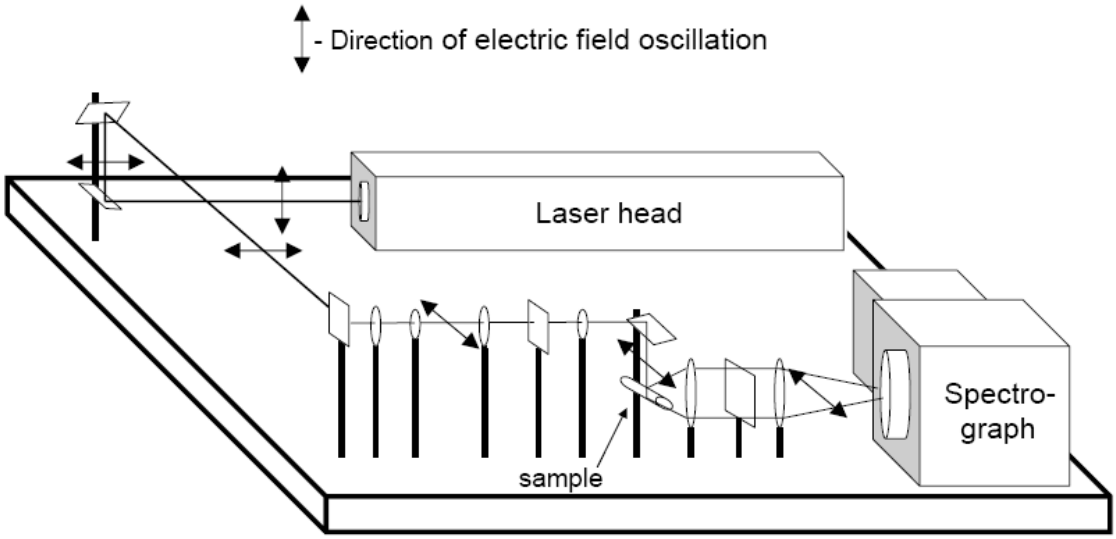

Figure 31: Diagrammatic representation of resonance Raman experimental setup. (courtesy Dr. James Terner)

A)

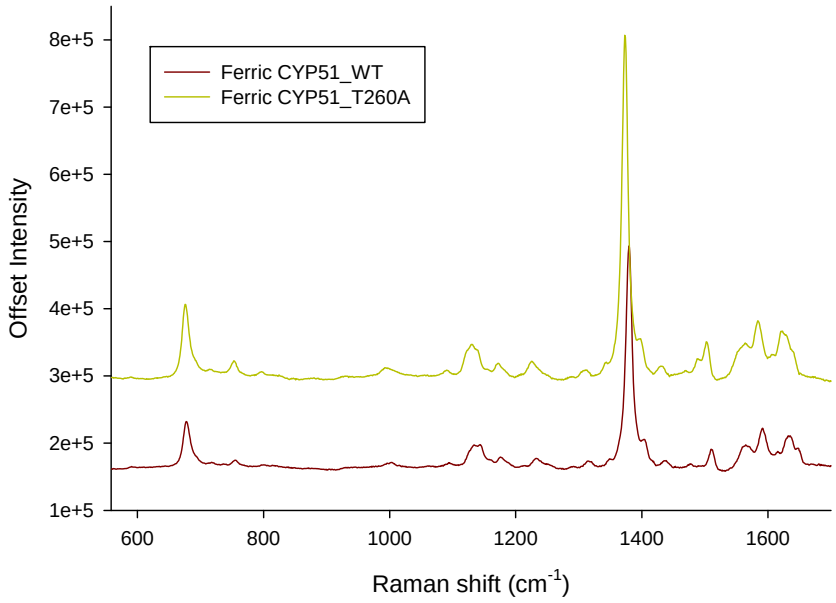

B)

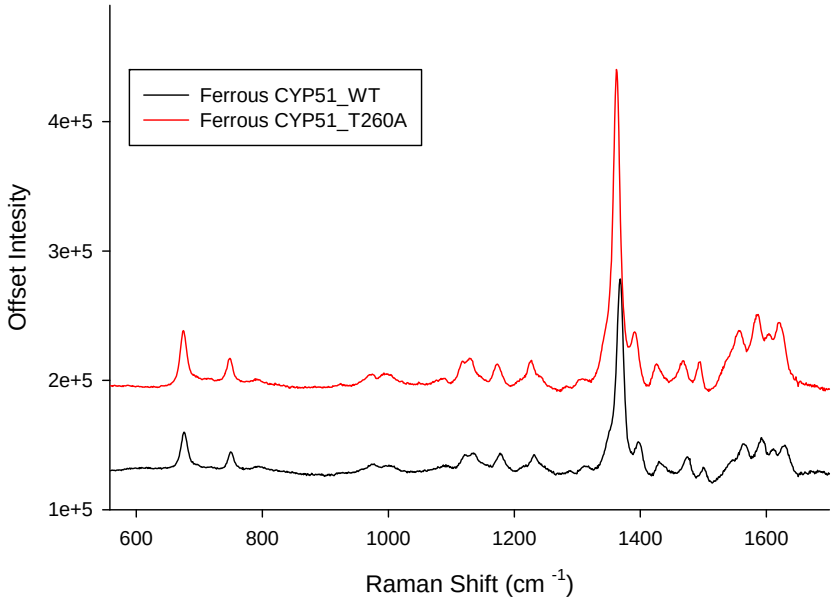

Figure 32: Resonance Raman spectra of A) ferric CYP51wt and T260A, B) ferrous CYP51wt and T260A.

A)

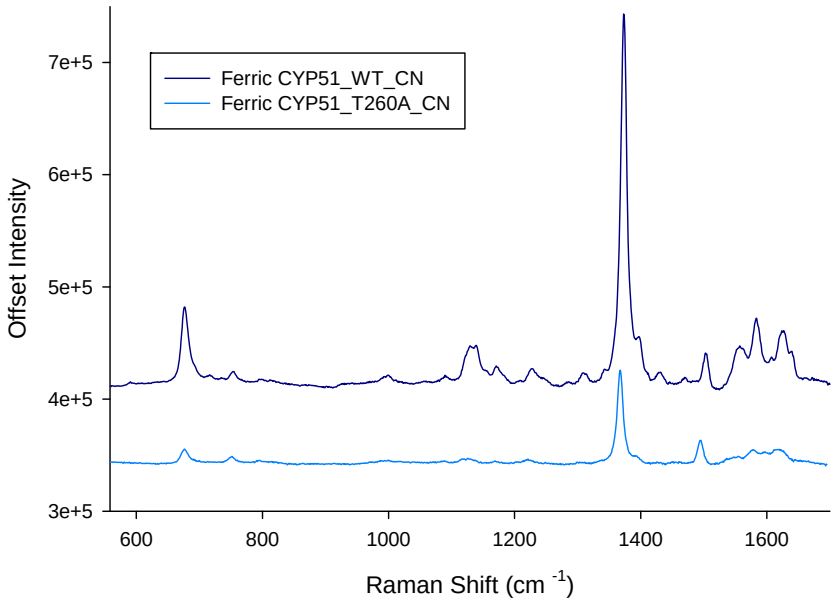

B)

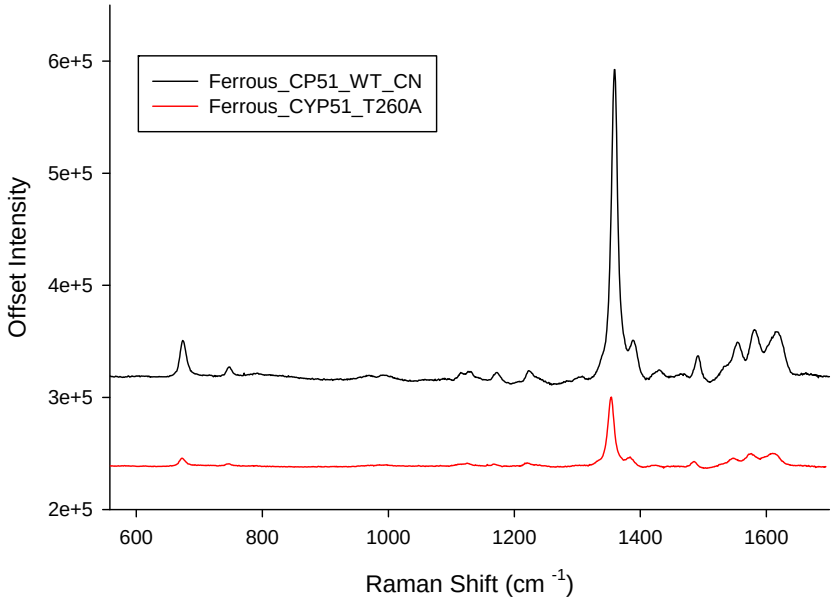

Figure 33: Resonance Raman spectra of A) ferric-CN CYP51wt and T260A, B) ferrous-CN CYP51wt and T260A.

A)

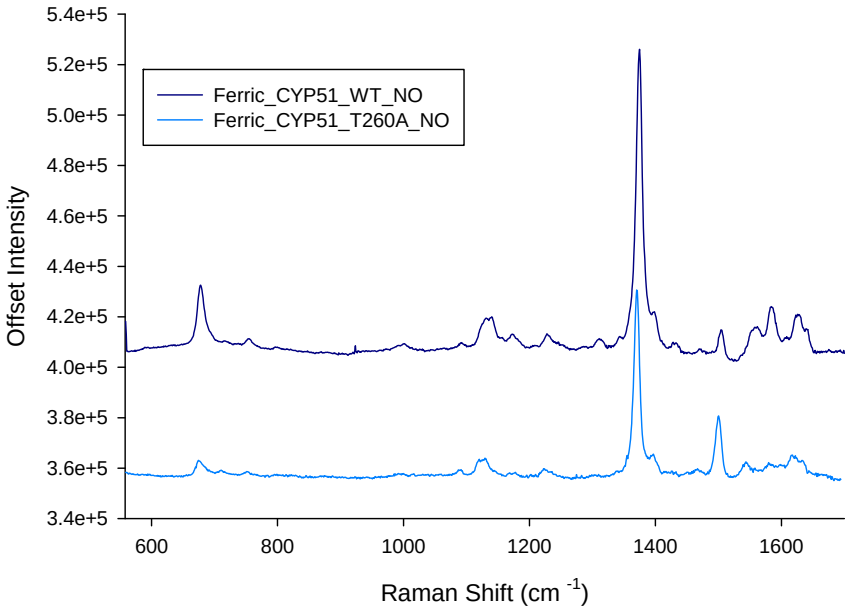

B)

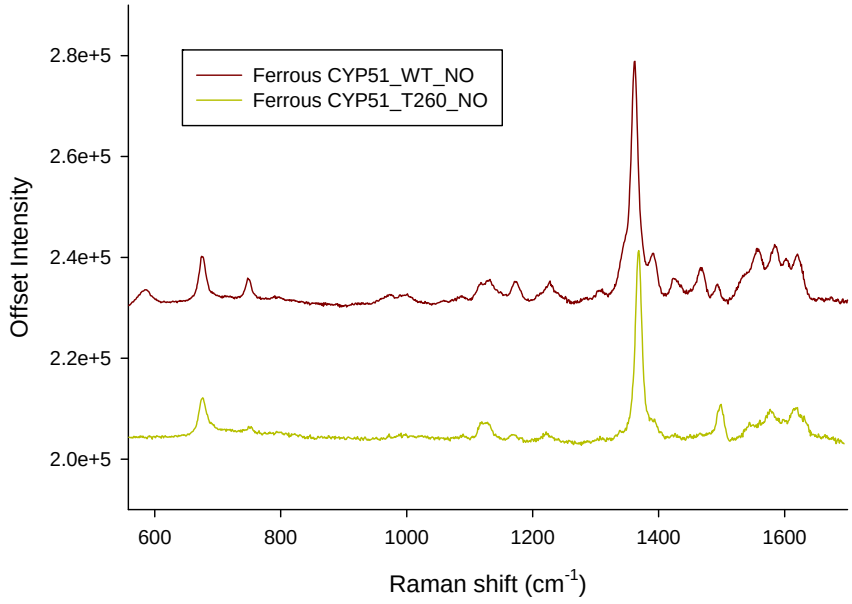

Figure 34: Resonance Raman spectra of A) ferric-NO CYP51wt and T260A, B) ferrous-NO CYP51wt and T260A.

Conclusions

1) CYP51wt and its mutants E173A, H259A and T260A which were made using site directed mutagenesis were successfully expressed. Their analysis by UV-vis spectroscopy gave information about their binding constants for the type I and type II ligands. It also indicated the unusual spectral characteristics of the T260A mutant.

2) Fdx, a conduit protein which is required to shuttle electrons for CYP51 catalysis was successfully cloned into pET46 Ek/LIC vector and expressed. Its spectral characteristics were similar as in published literature for other similar ferrdoxins. Fdx was found to support the electron transport chain to shuttle electrons from NADPH to CYP51wt as indicated by the ferrous-CO difference spectra.

3) Resonance Raman experiments revealed an interesting admixture of spin states in ferric T260A. This can be attributed to the loss of hydrogen bond between Thr260 and H_2O, thus causing the enzyme to exist in penta coordinate high spin form.

Bibliography:

1. Denisov, I. G.; Makris, T. M.; Sligar, S. G.; Schlichting, I. Structure and chemistry of cytochrome P450. *Chem. Rev.* **2005**, *105,* 2253-2277.

2. Rendic, S. Summary of information on human CYP enzymes: human P450 metabolism data. *Drug Metab. Rev.* **2002**, *34,* 83-448.

3. Miller, W. L. Steroidogenic enzymes. *Endocr Dev.* **2008**, *13,* 1-18.

4. Sono, M.; Roach, M. P.; Coulter, E. D.; Dawson, J. H. Heme-Containing Oxygenases. *Chem. Rev.* **1996**, *96,* 2841-2888.

5. Hayaishi, O. *Molecular mechanisms of oxygen activation;* Academic Press: New York, 1974; , pp 678.

6. Katagiri, M.; Ganguli, B. N.; Gunsalus, I. C. A soluble cytochrome P-450 functional in methylene hydroxylation. *J. Biol. Chem.* **1968**, *243,* 3543-3546.

7. Raj, P. P.; Nelson, E. B.; Estabrook, R. W. Studies on drug metabolism in human liver. *Chem. Biol. Interact.* **1971**, *3,* 303-304.

8. Lawson, R. J.; Leys, D.; Sutcliffe, M. J.; Kemp, C. A.; Cheesman, M. R.; Smith, S. J.; Clarkson, J.; Smith, W. E.; Haq, I.; Perkins, J. B.; Munro, A. W. Thermodynamic and biophysical characterization of cytochrome P450 BioI from Bacillus subtilis. *Biochemistry* **2004**, *43,* 12410-12426.

9. Sligar, S. G. Coupling of spin, substrate, and redox equilibria in cytochrome P450. *Biochemistry* **1976**, *15,* 5399-5406.

10. Davydov, R.; Perera, R.; Jin, S.; Yang, T. C.; Bryson, T. A.; Sono, M.; Dawson, J. H.; Hoffman, B. M. Substrate modulation of the properties and reactivity of the oxy-ferrous

and hydroperoxo-ferric intermediates of cytochrome P450cam as shown by cryoreduction-EPR/ENDOR spectroscopy. *J. Am. Chem. Soc.* **2005**, *127,* 1403-1413.

11. Denisov, I. G.; Mak, P. J.; Makris, T. M.; Sligar, S. G.; Kincaid, J. R. Resonance Raman Characterization of the Peroxo and Hydroperoxo Intermediates in Cytochrome P450. *J Phys Chem A* **2008**, .

12. John T. Groves, Gary A. McClusky Aliphatic hydroxylation via oxygen rebound. Oxygen transfer catalyzed by iron. *J. Am. Chem. Soc.* **1976**, *98,* 859-861.

13. Groves, J. T.; McClusky, G. A. Aliphatic hydroxylation by highly purified liver microsomal cytochrome P-450. Evidence for a carbon radical intermediate. *Biochem. Biophys. Res. Commun.* **1978**, *81,* 154-160.

14. Bernhardt, R. Cytochrome P450: Structure, function and generation of reactive oxygen species. *Rev. Physiol. Biochem. Pharmacol.* **1996**, *127,* 137-221.

15. Ortiz de Montellano, P. R. *Cytochrome P450 : structure, mechanism, and biochemistry;* Kluwer Academic/Plenum Publishers: New York, 2005; , pp 115.

16. Hiner, A. N.; Raven, E. L.; Thorneley, R. N.; Garcia-Canovas, F.; Rodriguez-Lopez, J. N. Mechanisms of compound I formation in heme peroxidases. *J. Inorg. Biochem.* **2002**, *91,* 27-34.

17. Fujii, H.; Zhang, X.; Tomita, T.; Ikeda-Saito, M.; Yoshida, T. A role for highly conserved carboxylate, aspartate-140, in oxygen activation and heme degradation by heme oxygenase-1. *J. Am. Chem. Soc.* **2001**, *123,* 6475-6484.

18. Groves, J. T.; Wang, C. C. Nitric oxide synthase: models and mechanisms. *Curr. Opin. Chem. Biol.* **2000**, *4,* 687-695.

19. John H. Dawson, Masanori. Sono Cytochrome P450 and chloroperoxidase: thiolate-ligated heme enzymes. Spectroscopic determination of their active site structures and mechanistic implication of thiolate ligation. *Chem. Rev.* **1987**, *87,* 1255-1276.

20. Nebert, D. W.; Nelson, D. R.; Coon, M. J.; Estabrook, R. W.; Feyereisen, R.; Fujii-Kuriyama, Y.; Gonzalez, F. J.; Guengerich, F. P.; Gunsalus, I. C.; Johnson, E. F. The P450 superfamily: update on new sequences, gene mapping, and recommended nomenclature. *DNA Cell Biol.* **1991**, *10,* 1-14.

21. Martinis, S.A., W.M. Atkins, P.S. Stayton, S.G. Sligar A conserved residue of cytochrome P450 is involved in heme-oxygen stability and activation. *J. Am. Chem. Soc.* **1989**, *111,* 9252-9253.

22. Vidakovic, M.; Sligar, S. G.; Li, H.; Poulos, T. L. Understanding the role of the essential Asp251 in cytochrome p450cam using site-directed mutagenesis, crystallography, and kinetic solvent isotope effect. *Biochemistry* **1998**, *37,* 9211-9219.

23. Gerber, N. C.; Sligar, S. G. A role for Asp-251 in cytochrome P-450cam oxygen activation. *J. Biol. Chem.* **1994**, *269,* 4260-4266.

24. Schlichting, I.; Jung, C.; Schulze, H. Crystal structure of cytochrome P-450cam complexed with the (1S)-camphor enantiomer. *FEBS Lett.* **1997**, *415,* 253-257.

25. Podust, L. M.; Yermalitskaya, L. V.; Lepesheva, G. I.; Podust, V. N.; Dalmasso, E. A.; Waterman, M. R. Estriol bound and ligand-free structures of sterol 14alpha-demethylase. *Structure* **2004**, *12,* 1937-1945.

26. Park, S. Y.; Yamane, K.; Adachi, S.; Shiro, Y.; Weiss, K. E.; Maves, S. A.; Sligar, S. G. Thermophilic cytochrome P450 (CYP119) from Sulfolobus solfataricus: high resolution structure and functional properties. *J. Inorg. Biochem.* **2002**, *91,* 491-501.

27. Girvan, H. M.; Seward, H. E.; Toogood, H. S.; Cheesman, M. R.; Leys, D.; Munro, A. W. Structural and spectroscopic characterization of P450 BM3 mutants with unprecedented P450 heme iron ligand sets. New heme ligation states influence conformational equilibria in P450 BM3. *J. Biol. Chem.* **2007**, *282,* 564-572.

28. Vergne, I.; Chua, J.; Singh, S. B.; Deretic, V. Cell biology of mycobacterium tuberculosis phagosome. *Annu. Rev. Cell Dev. Biol.* **2004**, *20,* 367-394.

29. Lee, R. E.; Brennan, P. J.; Besra, G. S. Mycobacterium tuberculosis cell envelope. *Curr. Top. Microbiol. Immunol.* **1996**, *215,* 1-27.

30. Laurenzi, M.; Ginsberg, A.; Spigelman, M. Challenges associated with current and future TB treatment. *Infect. Disord. Drug Targets* **2007**, *7,* 105-119.

31. Park, S. H.; Bendelac, A. CD1-restricted T-cell responses and microbial infection. *Nature* **2000**, *406,* 788-792.

32. Cole, S. T.; Brosch, R.; Parkhill, J.; Garnier, T.; Churcher, C.; Harris, D.; Gordon, S. V.; Eiglmeier, K.; Gas, S.; Barry, C. E.,3rd; Tekaia, F.; Badcock, K.; Basham, D.; Brown, D.; Chillingworth, T.; Connor, R.; Davies, R.; Devlin, K.; Feltwell, T.; Gentles, S.; Hamlin, N.; Holroyd, S.; Hornsby, T.; Jagels, K.; Krogh, A.; McLean, J.; Moule, S.; Murphy, L.; Oliver, K.; Osborne, J.; Quail, M. A.; Rajandream, M. A.; Rogers, J.; Rutter, S.; Seeger, K.; Skelton, J.; Squares, R.; Squares, S.; Sulston, J. E.; Taylor, K.; Whitehead,

S.; Barrell, B. G. Deciphering the biology of Mycobacterium tuberculosis from the complete genome sequence. *Nature* **1998**, *393,* 537-544.

33. McLean, K. J.; Munro, A. W. Structural biology and biochemistry of cytochrome P450 systems in Mycobacterium tuberculosis. *Drug Metab. Rev.* **2008**, *40,* 427-446.

34. Leys, D.; Mowat, C. G.; McLean, K. J.; Richmond, A.; Chapman, S. K.; Walkinshaw, M. D.; Munro, A. W. Atomic structure of Mycobacterium tuberculosis CYP121 to 1.06 A reveals novel features of cytochrome P450. *J. Biol. Chem.* **2003**, *278,* 5141-5147.

35. Ouellet, H.; Podust, L. M.; de Montellano, P. R. Mycobacterium tuberculosis CYP130: crystal structure, biophysical characterization, and interactions with antifungal azole drugs. *J. Biol. Chem.* **2008**, *283,* 5069-5080.

36. Waterman, M. R.; Lepesheva, G. I. Sterol 14 alpha-demethylase, an abundant and essential mixed-function oxidase. *Biochem. Biophys. Res. Commun.* **2005**, *338,* 418-422.

37. McLean, K. J.; Dunford, A. J.; Neeli, R.; Driscoll, M. D.; Munro, A. W. Structure, function and drug targeting in Mycobacterium tuberculosis cytochrome P450 systems. *Arch. Biochem. Biophys.* **2007**, *464,* 228-240.

38. Bellamine, A.; Mangla, A. T.; Nes, W. D.; Waterman, M. R. Characterization and catalytic properties of the sterol 14alpha-demethylase from Mycobacterium tuberculosis. *Proc. Natl. Acad. Sci. U. S. A.* **1999**, *96,* 8937-8942.

39. Gatfield, J.; Pieters, J. Essential role for cholesterol in entry of mycobacteria into macrophages. *Science* **2000**, *288,* 1647-1650.

40. McLean, K. J.; Cheesman, M. R.; Rivers, S. L.; Richmond, A.; Leys, D.; Chapman, S. K.; Reid, G. A.; Price, N. C.; Kelly, S. M.; Clarkson, J.; Smith, W. E.; Munro, A. W.

Expression, purification and spectroscopic characterization of the cytochrome P450 CYP121 from Mycobacterium tuberculosis. *J. Inorg. Biochem.* **2002**, *91,* 527-541.

41. Stewart, G. R.; Wernisch, L.; Stabler, R.; Mangan, J. A.; Hinds, J.; Laing, K. G.; Young, D. B.; Butcher, P. D. Dissection of the heat-shock response in Mycobacterium tuberculosis using mutants and microarrays. *Microbiology* **2002**, *148,* 3129-3138.

42. Kendall, S. L.; Rison, S. C.; Movahedzadeh, F.; Frita, R.; Stoker, N. G. What do microarrays really tell us about M. tuberculosis? *Trends Microbiol.* **2004**, *12,* 537-544.

43. Sassetti, C. M.; Boyd, D. H.; Rubin, E. J. Genes required for mycobacterial growth defined by high density mutagenesis. *Mol. Microbiol.* **2003**, *48,* 77-84.

44. Lepesheva, G. I.; Waterman, M. R. CYP51--the omnipotent P450. *Mol. Cell. Endocrinol.* **2004**, *215,* 165-170.

45. Akhtar, M.; Alexander, K.; Boar, R. B.; McGhie, J. F.; Barton, D. H. Chemical and enzymic studies on the characterization of intermediates during the removal of the 14alpha-methyl group in cholesterol biosynthesis. The use of 32-functionalized lanostane derivatives. *Biochem. J.* **1978**, *169,* 449-463.

46. Shyadehi, A. Z.; Lamb, D. C.; Kelly, S. L.; Kelly, D. E.; Schunck, W. H.; Wright, J. N.; Corina, D.; Akhtar, M. The mechanism of the acyl-carbon bond cleavage reaction catalyzed by recombinant sterol 14 alpha-demethylase of Candida albicans (other names are: lanosterol 14 alpha-demethylase, P-45014DM, and CYP51). *J. Biol. Chem.* **1996**, *271,* 12445-12450.

47. Sen, K.; Hackett, J. C. Molecular oxygen activation and proton transfer mechanisms in lanosterol 14alpha-demethylase catalysis. *J Phys Chem B* **2009**, *113,* 8170-8182.

48. Akhtar, M.; Calder, M. R.; Corina, D. L.; Wright, J. N. Mechanistic studies on C-19 demethylation in oestrogen biosynthesis. *Biochem. J.* **1982**, *201,* 569-580.

49. Akhtar, M.; Corina, D.; Miller, S.; Shyadehi, A. Z.; Wright, J. N. Mechanism of the acyl-carbon cleavage and related reactions catalyzed by multifunctional P-450s: studies on cytochrome P-450(17)alpha. *Biochemistry* **1994**, *33,* 4410-4418.

50. Lambeth, J. D.; Kitchen, S. E.; Farooqui, A. A.; Tuckey, R.; Kamin, H. Cytochrome P-450scc-substrate interactions. Studies of binding and catalytic activity using hydroxycholesterols. *J. Biol. Chem.* **1982**, *257,* 1876-1884.

51. Schlichting, I.; Berendzen, J.; Chu, K.; Stock, A. M.; Maves, S. A.; Benson, D. E.; Sweet, R. M.; Ringe, D.; Petsko, G. A.; Sligar, S. G. The catalytic pathway of cytochrome p450cam at atomic resolution. *Science* **2000**, *287,* 1615-1622.

52. Nagano, S.; Cupp-Vickery, J. R.; Poulos, T. L. Crystal structures of the ferrous dioxygen complex of wild-type cytochrome P450eryF and its mutants, A245S and A245T: investigation of the proton transfer system in P450eryF. *J. Biol. Chem.* **2005**, *280,* 22102-22107.

53. Park, S. Y.; Yamane, K.; Adachi, S.; Shiro, Y.; Weiss, K. E.; Maves, S. A.; Sligar, S. G. Thermophilic cytochrome P450 (CYP119) from Sulfolobus solfataricus: high resolution structure and functional properties. *J. Inorg. Biochem.* **2002**, *91,* 491-501.

54. Podust, L. M.; von Kries, J. P.; Eddine, A. N.; Kim, Y.; Yermalitskaya, L. V.; Kuehne, R.; Ouellet, H.; Warrier, T.; Altekoster, M.; Lee, J. S.; Rademann, J.; Oschkinat, H.; Kaufmann, S. H.; Waterman, M. R. Small-molecule scaffolds for CYP51 inhibitors

identified by high-throughput screening and defined by X-ray crystallography. *Antimicrob. Agents Chemother.* **2007**, *51,* 3915-3923.

55. Bradford, M. M. A rapid and sensitive method for the quantitation of microgram quantities of protein utilizing the principle of protein-dye binding. *Anal. Biochem.* **1976**, *72,* 248-254.

56. Recchi, C.; Sclavi, B.; Rauzier, J.; Gicquel, B.; Reyrat, J. M. Mycobacterium tuberculosis Rv1395 is a class III transcriptional regulator of the AraC family involved in cytochrome P450 regulation. *J. Biol. Chem.* **2003**, *278,* 33763-33773.

57. Schenkman, J. B.; Jansson, I. Spectral Analyses of Cytochromes P450. In *Cytochrome P450 Protocols;* 2005; Vol. 320, pp 11-18.

58. OMURA, T.; SATO, R. The Carbon Monoxide-Binding Pigment of Liver Microsomes. I. Evidence for its Hemoprotein Nature. *J. Biol. Chem.* **1964**, *239,* 2370-2378.

59. Salmon, F.; Taton, M.; Benveniste, P.; Rahier, A. Plant sterol biosynthesis: novel potent and selective inhibitors of cytochrome P450-dependent obtusifoliol 14 alpha-methyl demethylase. *Arch. Biochem. Biophys.* **1992**, *297,* 123-131.

60. Yoshida, Y.; Aoyama, Y. Interaction of azole antifungal agents with cytochrome P-45014DM purified from Saccharomyces cerevisiae microsomes. *Biochem. Pharmacol.* **1987**, *36,* 229-235.

61. McLean, K. J.; Warman, A. J.; Seward, H. E.; Marshall, K. R.; Girvan, H. M.; Cheesman, M. R.; Waterman, M. R.; Munro, A. W. Biophysical characterization of the sterol demethylase P450 from Mycobacterium tuberculosis, its cognate ferredoxin, and their interactions. *Biochemistry* **2006**, *45,* 8427-8443.

62. C.V Raman and K.S Krishnan. *A New Type of Secondary Radiation*. *Nature* **1928**, *121,* 501-502.

63. Smith, E.; Dent, G. *Modern Raman spectroscopy : a practical approach;* J. Wiley: Hoboken, NJ, 2005; , pp 210.

64. Spiro, T. G. *Resonance Raman spectra of Heme and metalloproteins;* Wiley: New York, 1988; Vol. 3, pp 565.

VITA

Anuja R. Modi was born on 4th October 1985, in Mumbai, India. Anuja graduated from D. G Ruparel Junior college in 2003. She matriculated to Bombay College of Pharmacy; Mumbai University in 2003.and received her Bachelor of Pharmaceutical Sciences degree in 2007. During the course of her B. Pharm. Sci. degree she presented a poster titled "Trends in Antibiotic/Antimicrobial Therapy for Pediatric Patients" for the National Poster Competition at 57th Indian Pharmaceutical Congress, Hyderabad, India. As a part of her curricular training for the B. Pharm. Sci. she worked in Sun Pharmaceutical Industries Limited at Mumbai, India for a month in May 2006. In the fall of 2007 she joined the Medicinal Chemistry Department at Virginia Commonwealth University to pursue the M.S. degree in Pharmaceutical Sciences.